journal of the international meteor organization

WGN

50:3-4
jun.-aug. 2022

In memoriam: Jean-Louis Rault and Jeff Brower
Radio and video observations combined
2022 May shower performance overview
Tau Herculids: observations and results

ISSN 1016-3115

WGN Vol. 50, No. 3–4, June–August 2022, pp. 71 – 108

Administrative

Ongoing Meteor Work

Tau Herculids

Front cover photo

Horizontal fireball captured with an AllSky7 Camera System on 2022 April 17 at $19^{h}48^{m}$ UT from Brandenburg, Germany.
For more information on this fireball visit: `https://fireball.imo.net/members/imo_view/event/2022/2411`
Photo courtesy: Sirko Molau.

Writing for WGN

This Journal welcomes papers submitted for publication. All papers are reviewed for scientific content, and edited for English and style. Instructions for authors can be found in WGN **45:1**, 1–5, and at `http://www.imo.net/docs/writingforwgn.pdf` .

Legal address

International Meteor Organization, Jozef Mattheessensstraat 60, 2540 Hove, Belgium.

From the Editor-in-Chief

Javor Kac

This July we sadly lost our friend Jean-Louis Rault, long-time WGN Editorial Board and IMO Council member and Director of the Radio Commission. Our organization is much indebted to Jean-Louis, and we will miss him dearly. We convey our condolences to his family. IMO Council member Karl Antier wrote Jean-Louis's obituary which you can read in the following pages. Unfortunately, we also lost our long-time radio observer Jeff Brower for whom Chris Steyaert wrote an obituary.

Many of you might have noticed the delays in WGN publication over the past couple of months. This comes as a result of very few submissions to WGN in the last year. I hope this was related to COVID restrictions and lack of personal contact during this period, and that this situation will improve in the near future.

Luckily, we have compiled enough articles to publish a double issue, in order to come back on track. This includes a number of reports and analyses of the recent Tau Herculid outburst. I hope you will enjoy reading this issue.

However, as any other journal, WGN can only publish papers submitted to our Journal. I would therefore like to invite you again to write and submit your meteor-related work for publication in WGN. All kinds of meteor-related articles are welcome.

IMO bibcode WGN-503–4-kac-editorial NASA-ADS bibcode 2022JIMO...50...71K

In memoriam: Jean-Louis Rault (10/03/1949 – 21/07/2022)

Karl Antier[1]

Received 2022 September 4

On July 21st, 2022, French amateur radio-astronomer and former Council Member of the IMO Jean-Louis Rault passed away.

Jean-Louis Rault was born March 30, 1949 in Saigon (Vietnam) from parents who were pharmacists practicing in the Army Health services. After being diagnosed with a double bronchopneumonia that nearly killed him and left him very weak, a doctor told her mother it was "criminal to let him live under such a climate". Decision was taken to send him to France and thus to separate him from his parents. He celebrated his first birthday in the plane flying him to Brittany, where her grandmother retired beforehand of time from her work as a teacher to raise him in Brest for 2 years, until his parents finished their assignment in Saigon.

A few years later, while he was 8 years old, a global event was to trigger his passion for astronomy (and probably radio-astronomy): during a radio transmission, in October 1957, he heard the "bip-bip" signal from the first artificial satellite, Sputnik. This initiated in him 65 years of astronomical, scientific and technical passions!

Fourteen years later and after learning electronics, he was expected to do his the national military service, but he volunteered as a civil technical aid to avoid playing at war and to enhance his technical skills. This decision led to an important step in Jean-Louis's life and scientific future, as he spent 2 years in the French Southern and Antarctic Lands (Figure 1). While working for mission #23 (1973–1975) in this territory, he started working on Very Large Frequency wavelengths, especially on sudden ionospheric disturbances. A scientific domain on which he would go on working all his life. At the end of the mission, he stayed another summer semester in the Kerguelen Island, as he was not really in a hurry to come back to France. On the way back, he worked for a few months in Madagascar at the Tananarive Observatory, where, again, he nearly died after having contracted typhoid fever.

Figure 1 – September 1973, Jean-Louis Rault working in B6 laboratory during his civil volunteering journey as technical aid in Kerguelen island for mission #23.

Jean-Louis graduated from the École centrale d'Électronique (Electronics central engineering School), located in rue de la Lune (Moon Street), in Paris. A diploma that led him to go back in Austral territories, but mainly in oceans, to work on oil & gas producing platforms and vessels, on which he was in charge of the electronics

[1]Email: karl.antier@protonmail.com

and informatics to position and stabilize them, in spite of the currents and the swell. He later worked for Thales defense systems as a Development Engineer and Program Manager for international contracts.

Living his passion for radio-astronomy and amateur sciences, willing to show even amateurs can direct big projects, Jean-Louis joined many associations and programs. As secretary, treasurer and President of AMSAT-France, he succeeded in developing 4 amateur satellites (Spoutnik 40 & 41, Idéfix 1 & 2) that were launched by the MIR station and Ariane 4 launchers. This may explain why he was proposed as technical advisor for the radio communication systems of the satellite programs Meteor (IMCCE) and Picsat (LESIA) of Paris Observatory.

His methods for observing meteors using radio detection are also demonstrated by his membership in the Société Astronomique de France (SAF, French Astronomical Society), for which he directed the radio-astronomy section from 2008 to 2019. Also known as F6AGR, he was a member of the REF (Réseau des Émetteurs Français) as a radio amateur and participated in the Radio-REF Journal Technical Committee. All meteor observers who practice their activities in Western Europe know the BRAMS (Belgian RAdio Meteor Stations) network, in which he also was engaged. One cannot forget his devotion to animating numerous mailing lists regarding radio astronomy, ELF, VLF and meteor astronomy.

Jean-Louis joined the International Meteor Organization in 2006. The year after, he became Head of the Radio Commission, for which he was responsible until 2021, and he was also part of the Council of the IMO from 2014 to 2021. He was one of the persons that would never miss an International Meteor Conference (Figure 2), as he assisted to all of them from 2007 to 2019 (except in 2018, when he had to take care of his wife who had broken her leg as they were spending holidays in a lost countryside of Corrèze to observe meteors in radio, ELF and VLF). He was co-editor of the IMC Proceedings in 2014, 2015 and 2017, and the author and co-author of numerous papers published in WGN (the Journal of the IMO), Astronomy & Astrophysics and other scientific journals.

Figure 2 – Jean-Louis Rault (right) chairing the radio session in the 2019 International Meteor Conference in Bollmannsruh, Germany. Credit: Mariusz Wiśniewski.

Once retired, he spent a lot of his energy working with the National Museum of Natural History and the Paris Observatory to work on a brand-new meteor observing network, FRIPON (Fireball Recovery and InterPlanetary Observation Network), for which he was in charge of the radio system development, implementation and data processing. At the same time, he contributed to the sister citizen science program Vigie-Ciel.

Discovered on June 25, 1998, by the OCA-DLR Asteroid Survey (ODAS) using a 90 cm-diameter Schmidt telescope on the Calern plateau Observatory (Caussols), minor planet 40081 (1998 MG14) has been named after Jean-Louis. With a 14.76 absolute magnitude, this asteroid is about 4 km in diameter.

Figure 3 – Jean-Louis Rault, tireless enthusiast radio-astronomer, in 2016. Credit: Danièle Rault.

WGSBN official bulletin

(40081) Rault = 1998 MG14
Discovery: 1998-06-25 / ODAS / Caussols / 910
Jean Louis Rault (b. 1949) is a French amateur radio astronomer who was president of the radioastronomy commission of the Société Astronomique de France from 2008 to 2019. He is responsible for the radio part of the Vigie-Ciel network, which detects the echoes of the GRAVES space surveillance radar.

Jean-Louis always transmitted his knowledge to people, from pupils to researchers, with passion and humor. We lost a big IMO supporter and a dear friend.
In the name of the meteor community, we send our sincere condolences to his family.

IMO bibcode WGN-503–4-antier-rault NASA-ADS bibcode 2022JIMO...50...72A

In memoriam: Jeff Brower 1948 – 2022

Chris Steyaert[1]

Received 2022 August 26

I came in contact with Jeff some 20 years ago via `rmob.org`. As a radio amateur, Jeff was wondering if more could be done with meteor scatter observations than casual reports. That challenge was taken on, and resulted in several studies that are complementary to the optical ones.

Since then we were in contact every month when he submitted his observations, and we talked private life and the situation in the world. Soon he became an IMO member.

For Jeff, his interest was 'everything flying in the sky', and beyond. Our last long exchange was in the fall of 2021 about the Cumbre Vieja volcanic eruption on La Palma. He and his wife Annette visited that area at the occasion of the 2012 IMC. It was their intention to attend more IMCs, but COVID jeopardized the plans.

With Jeff we lose a member of the IMO family and a man of science, much needed nowadays.

Figure 1 – Jeff and Annette at La Palma in 2012. Photo courtesy: Chris Steyaert.

Figure 2 – Jeff & Chris at La Palma in 2012. Photo courtesy: Annette Brower.

Figure 3 – Jeff and Arnaud Leroy at La Palma in 2012. Photo courtesy: Chris Steyaert.

Figure 4 – Jeff & Chris at La Palma in the GTC 2012. Photo courtesy: Annette Brower.

IMO bibcode WGN-503–4-steyaert-brower NASA-ADS bibcode 2022JIMO...50...75S

[1]Email: `csteyaert@gmail.com`

Ongoing Meteor Work

What we can record by radio meteor observations—findings by collation with video observations

Masahiro Koseki[1] *and Kenji Fujito*[2]

We tried to collate Ham-band Radio Observations of meteors (HRO) with video observations (SonotaCo net). We found the inner product (*IP*) between a meteor path and the ellipsoid having focuses of the transmitter and the receiver plays a very important role in HRO. It is suggested that the following four conditions could be used as the standard for the collation.
(1) The time lag Δt could not be longer than 10 seconds no matter how large *IP* is.
(2) *IP* might not be larger than 0.5 when the distance $D = R_1 + R_2 < 500$ km, though $IP > 0.5$ is acceptable at nearer D.
D is the sum of the ranges from the emitter to the middle point of the meteor and from the latter to the receiver ($R_1 + R_2$ of Figure 2).
(3) Meteors of fainter than $-3^{\rm rd}$ magnitude could not be detectable when $D > 600$ km.
(4) The farther the distance, the weaker the intensity; the echoes could not be detectable farther than $D > 1000$ km.
We estimated the electron line density from the video absolute magnitude and found that HRO can record $5^{\rm th}$ to $6^{\rm th}$ video magnitude meteors. HRO records overdense echoes mainly but can catch underdense echoes when they appear near the sites; the border of overdense echoes and underdense ones may lie in $4^{\rm th}$ to $5^{\rm th}$ magnitude.
We calculated the ceiling height expressed by McKinley (1961) and found HRO is hindered in case of fast meteors specifically for Orionids. The midpoints of their paths change with radiant altitude; the lower the radiant, the higher the midpoint. When the radiant is at 10 degrees the midpoint of Orionids would be above the ceiling height and when 70 degrees, under it. Geminids are slower than Orionids and all meteors appear below the ceiling height. It is necessary to compensate Orionid echo numbers by the radiant altitude, though not for Geminids.
HRO can record meteors in the range of visual observations. If we could compensate unique influences in radio observations, HRO can give good profiles of meteor activities without the obstruction of weather and daylight.

Received 2022 May 16

1 Introduction

Ham-band Radio Observations of meteors (hereafter HRO) in Japan owe much to voluntary transmissions. Ogawa (2022) introduces Japanese HRO and opens the newest observations. It seems to be unnecessary to describe ordinary observational techniques in HRO here.

We can count echo numbers from radio recordings but can also get more information from them. It is very interesting to compare HRO with video observations; SonotaCo net provides many useful data in Japan, especially for the central area of Japan (SonotaCo, 2009).

One of the authors, Fujito, had started HRO since 2002 November and SonotaCo net had been publishing video data since 2007. We investigate 2009 Orionids and 2018 Geminids in this paper; observational conditions were good in both years. We used different transmissions, SABAE for Orionids and FUKUI for Geminids because the former transmitter (SABAE) stopped in 2018 and the new one (FUKUI) succeeded.

[1]The Nippon Meteor Society, 4-3-5 Annaka, Annaka-shi, Gunma, 379-0116 JAPAN. Email: geh04301@nifty.ne.jp
[2]The Nippon Meteor Society, 4-6 Minamihamada, Yokkaichi, Mie, 510-0066 JAPAN

IMO bibcode WGN-503–4-koseki-radiovideo
NASA-ADS bibcode 2022JIMO...50...76K

Receiver and transmitter details:
– SABAE: 136.17E, 35.94N, 53.750MHz, vertical, 2 polarization planes, 50W
– FUKUI: 136.28E, 36.11N, 53.755MHz, vertical, 2 polarization planes, 50W
– YOKKAICHI: 136.61E, 34.96N
Distances: SABAE-YOKKAICHI = 115.4 km, FUKUI-YOKKAICHI = 130.8 km

The receiver (YOKKAICHI) locates south of both transmitters and Fujito at YOKKAICHI can record shower activities at their culmination (maximum altitude) of the radiant almost along the transmitter–receiver line (Figure 1).

2 Basic conditions of our HRO

Meteor echoes are perceptible in the case of meteor paths lying on an ellipsoid that has focuses on the emitter and the receiver. Figure 2 shows the ellipsoids and meteor paths which could be caught as meteor echoes in the case of our study. The right cross indicates the emitter (SABAE or FUKUI) and the left the receiver (Fujito, YOKKAICHI). In this figure, meteor paths begin at 100 km above the ground and end at 80 km and we ignore the sphere of the Earth hereafter.

We know we can record meteor echoes even its path crosses the ellipsoid. It is necessary to express the angle between them to know we can and cannot receive echoes

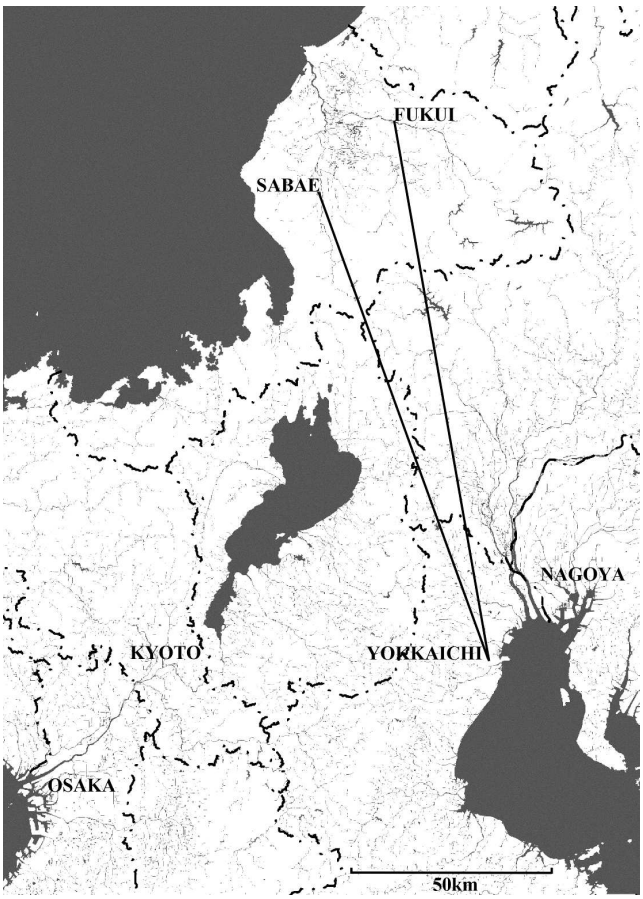

Figure 1 – The locations of the transmitters (SABAE and FUKUI) and the receiver (YOKKAICHI).

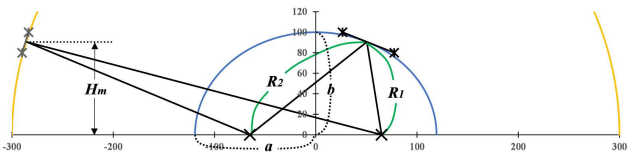

Figure 2 – The scheme of the reflection of the radio wave by meteor paths along with the ellipsoid.

depending on how deeply the meteor path intersects the ellipsoid. We introduce the inner product between a meteor path and the plane of the ellipsoid (hereafter IP, Figure 3).

When we set direction cosines of a meteor and the normal line of the ellipsoid (Lx, Ly, Lz) and (lx, ly, lz) respectively, we can easily calculate IP as follows; the ellipsoid is adopted to the middle point of the meteor path. $IP = Lxlx + Lyly + Lzlz = \cos\theta$

3 Orionids and Geminids: high and moderate velocity meteor showers

It is useful to realize the difference between HRO and video observations by comparing meteor showers of different geocentric velocity. Koseki (2015) confirmed how meteor showers are determined differently by different observational techniques. Radio observations favor in meteors with middle range velocity, and video observations meteors with high velocity. We choose Orionids and Geminids as the reference; Geminids are one of the

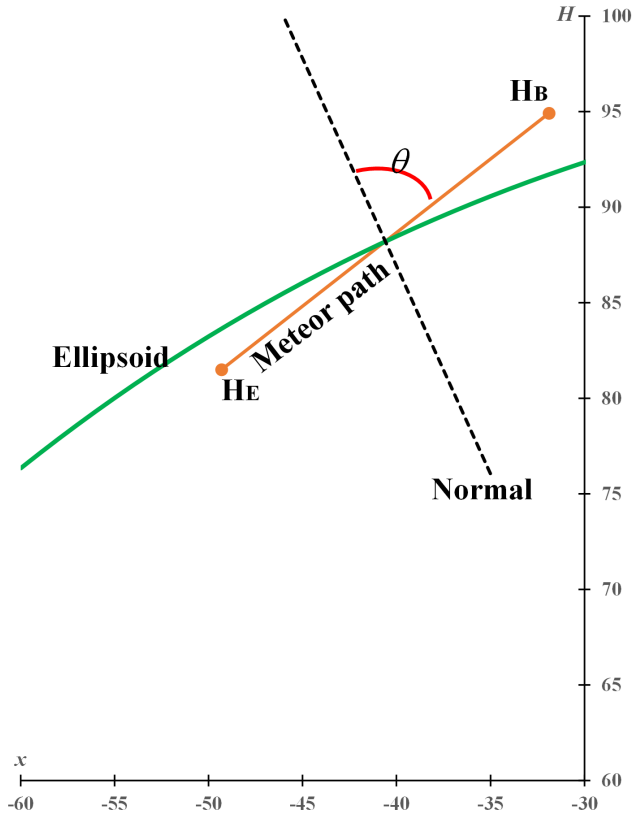

Figure 3 – The inner product $IP = \cos\theta$ between a meteor path and the ellipsoid.

major showers and moderate velocity, and Orionids are rapid on the other hand. Both shower radiants pass the culmination and their radiants climb up to more than 70 degrees in Japan, though Perseids are hindered by morning twilight and their culmination cannot be pursued by video observations.

Geminids are the strongest meteor shower during the year and Orionids are weaker though one of the major showers. Hourly meteor rates at their maximum of Geminids surpass Orionids several times in regular years. We had witnessed rare, enhanced activities of Orionids in 2007 to 2009 and their hourly meteor rates became comparable with Geminids (Figure 4a). We use 2009 Orionids observations of October 20–22 and 2018 Geminids of December 13–15 to compare their characteristics. We treat all records including members of sporadic and other minor meteor showers as Orionids or Geminids in this section, because we have not collated HRO with video observations yet (see next Section).

3.1 Meteor rates of Orionids and Geminids

Figure 4a shows the moving mean 10 minute rates of video meteors in 30 minute bins starting from October 21, 22:00 (JST=UTC+9) for Orionids and December 14, 19:00 (JST) for Geminids. It is clear Orionids were as active as Geminids then and Geminid activity decreases after its culmination: after 200 minutes from the beginning of the counting ordinarily.

Figure 4b displays the radio rates and we can easily notice the complex conditions of radio meteor observations. Geminid activity shows a basin around the

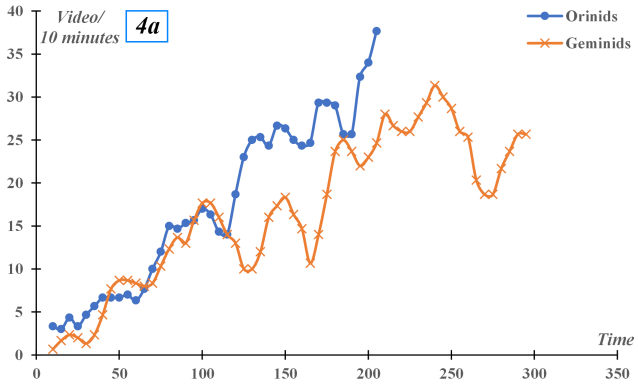

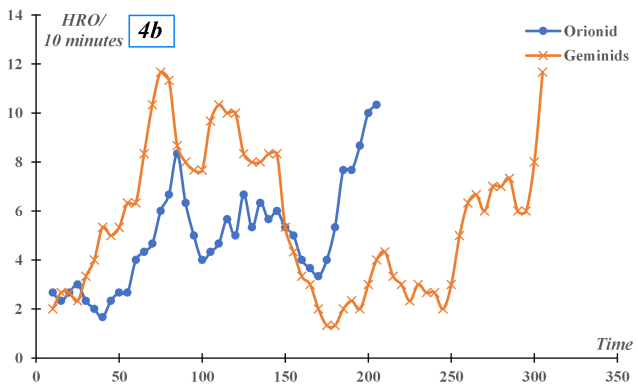

Figure 4 – a.) The moving mean 10 minute rates of video meteors in 30 minute bin starting from 2009 October 21, $22^{h}00^{m}$ (JST=UTC+9), for Orionids and 2018 December 14, $19^{h}00^{m}$ (JST=UTC+9), for Geminids. b.) Orionids and Geminids by HRO figured as the same manner in Figure 4a.

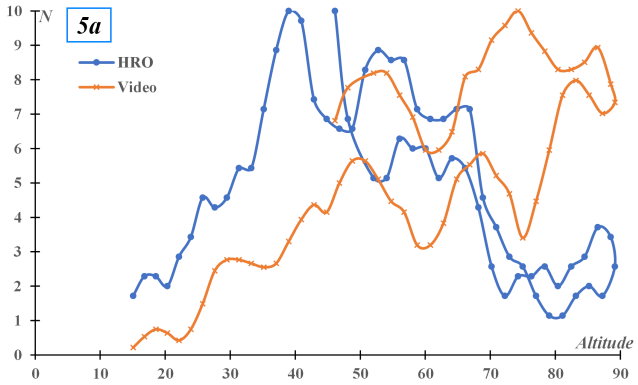

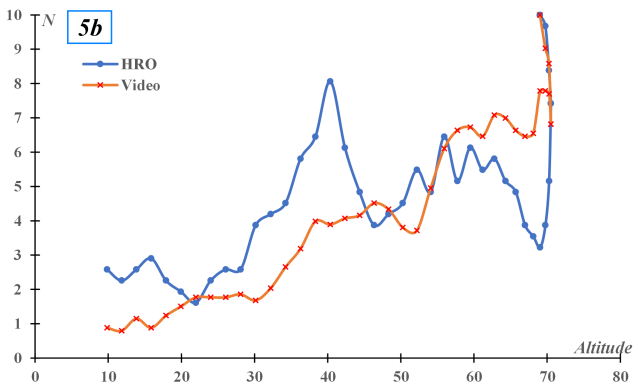

Figure 5 – a.) The normalized 10 minute rates (the maximum set to 10) of Geminids along with the radiant altitude. b.) The normalized number (the maximum set to 10) of Orionids along with the radiant altitude.

culmination of the radiant; this is very usual in radio meteor observations (see Section 4.3. The differences between Orionids and Geminids). Orionids give lower rates than Geminids before Time < 150; though they are almost the same in video observations (Figure 4a and see Figure 7 also).

3.2 Comparison between video and HRO

We normalized the maximum 10 minute rates shown in Figure 4a and 4b to 10 to compare the change of HRO and video rates in Geminids along with the radiant altitude (Figure 5a). HRO rates have a peak around 40 degrees and decrease toward the culmination. After the culmination the Geminid radiant goes down and HRO rates increase again, though video rates reach a maximum around the culmination.

Figure 5b shows the normalized rates (the maximum set to 10) of Orionids. It is worth noticing the numbers happen to rise suddenly after the culmination, that is, about 70 degrees. This is a mini outburst of Orionids because both echoes and videos recorded the event.

The number of echoes has a peak around 40 degrees as Geminids do but does not so deeply decrease as Geminids. This is a curious phenomenon indeed as shown in the next section. On the other hand, video meteors increased to the culmination of the radiant naturally.

3.3 Comparison between Orionid and Geminid echoes

We can get other information concerning individual echoes; the intensity and the duration from the bar chart on the screen (see Figure 9 inset). The screen is redrawing every 1 second and the duration cannot be measured on a short scale. It is natural that the detectable echo intensity changes with the background noise, but the background noise is stable in our search period, and we can detect weak echoes of intensity 5–6 at its best.

We compare Orionids with Geminids by using observations 2009 October 21, 22:00 to October 22, 05:00 for Orionids and 2018 December 14, 19:00 to December 15, 05:00 for Geminids; we use all video meteors here because HRO cannot distinguish shower meteors from sporadic meteors. Figure 6a–c exhibit the percentage of the total meteors observed in each period given above.

Figures 6a and 6b show frequency distributions of the duration and the intensity respectively. The duration of the overwhelming majority of Orionids is only 1 second and the percentages of Orionids weaker than 10 in intensity are 1.5 times larger than those of Geminids. Figure 6c represents the absolute magnitude distribution of video meteors by a moving mean over 0.5 magnitude bins and shows there is no cause in video for such differences in HRO. We can confirm that echoes of Orionids are weaker and shorter than Geminids ones.

The most interesting difference between HRO and video observations is the shift of the ratio of echoes

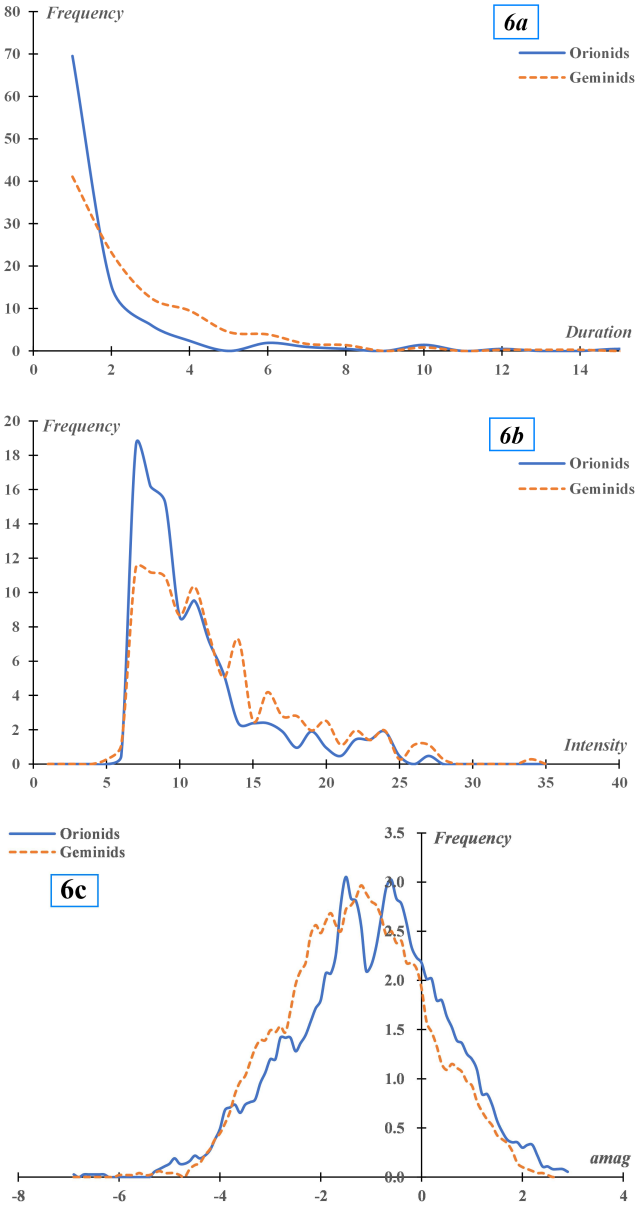

Figure 6 – a.) Comparison between Orionids and Geminids in the echo duration. b.) Comparison between Orionids and Geminids in the echo intensity. c.) Absolute magnitude distribution of video meteor by moving mean of 0.5 magnitude bin.

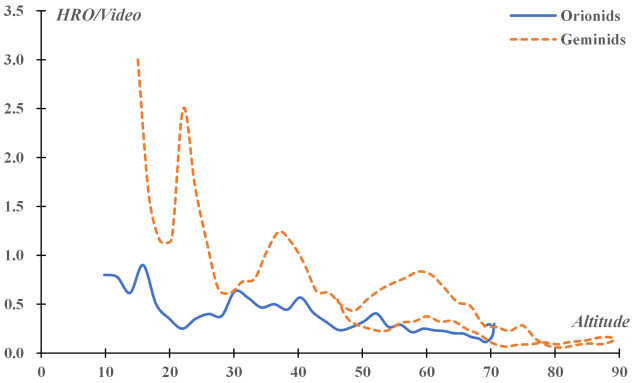

Figure 7 – Comparison between Orionid and Geminid rates in the ratio of HRO rates to video rates against radiant altitude.

to video meteors with the altitude of the radiant (Figure 7). The ratio of Geminids decreases with the altitude of the radiant because the distance from the stations increases with the altitude (see Figure 2). This tendency is weak in Orionids and, moreover, the ratio is almost below Geminids, though both video rates are almost the same as shown in Figure 4a. We will return to this interesting finding in Section 6 (Orionids and the ceiling height).

4 Collation with video observations

4.1 Standard for collation: typical echoes

It is proper to collect sure examples of the combination of the simultaneous records to outline the standard for collation at first. Orionids leave impressive trains sometimes and we chose 17 strong echoes in the period of our investigation (Table 1 and Figure 8a to 8d). It seems to be easier to study Orionids' case firstly to settle the standard; Geminids are not suitable for this purpose (see the last part of this section).

We can suggest the following 4 standards to collate echoes with video observations based on Figures 8a to 8d.

1. The time lag Δt could not be longer than 10 seconds no matter how large IP is.

   It is very clear the time lag Δt becomes longer when the intersection angle, that is abs(IP), is large (Figure 8a); the time lag may be caused by the necessary time to disperse the reflective matter: mainly electrons. We can collate echoes with video observations using this relation; Δt would be short when IP is small and vice versa. It is suggested Δt might not become longer than 10 seconds.

2. IP might not be larger than 0.5 when the distance $D = R_1 + R_2 > 500$ km, though $IP > 0.5$ is acceptable at nearer D.

   It is also clear that we cannot receive echoes from meteors rushing into the ellipsoid with large angle when the distance from the observational sites becomes farther (Figure 8b). IP should be less than 0.5, that is, an intersection angle of 30 degrees against the ellipsoid, though we could catch echoes of $IP > 0.5$ if $D < 500$ km when the electrons are dispersed enough. We can reject seeming coincident pairs of echoes and videos.

3. Meteors of fainter than -3 magnitude could not be detectable when $D > 600$ km.

   We can add one more criterion to refine the list of the candidates of the collation. It is a very natural condition; when the distance from the sites becomes farther, we cannot receive echoes from fainter meteors (Figure 8c). When the distance from the sites $(R_1 + R_2)$ is longer than 600 km, we cannot perceive the echoes fainter than -3 magnitude.

Table 1 – Remarkable echoes and identified video observations in 2009 October 20–22. HRO is the starting time of the echo, I is the intensity of the echo, $Dur.$ is the duration of the echo, Video is the time of the video observations, Δt is the time lag, that is, difference in two observations: HRO-Video, M_a is the absolute magnitude, abs(IP) is the absolute IP, $90-\theta$ is the angle between the ellipsoid and the meteor path, D is the distance of the sum of the ranges from the emitter to the middle point of the meteor and from the latter to the receiver (R_1+R_2 of Figure 2), class is the shower name classified by SonotaCo net. *1 and *2 have other candidates showing in the last two lines.

Date	HRO	I	$Dur.$	Video	Δt	M_a	abs(IP)	$90-\theta$	D	class
10/20	005232	21	23	005230	2	−4.0	0.114	6.6	336	ORI
	053104	28	67	053101	3	−3.8	0.150	8.6	377	ORI
10/21	004220	17	20	004219	1	−3.2	0.426	25.2	279	ORI
	004504	30	7	004503	1	−2.3	0.076	4.4	298	ORI
	015613	15	45	015606	7	−4.7	0.482	28.8	470	ORI
	025214	18	51	025210	4	−6.0	0.249	14.4	485	ORI*1
	033929	31	15	033929	0	−1.6	0.047	2.7	308	SPO
	035438	27	57	035435	3	−5.5	0.154	8.9	454	ORI
	045927	21	28	045925	2	−3.8	0.099	5.7	452	ORI*2
10/22	012428	27	35	012428	0	−4.3	0.018	1.0	376	ORI
	020110	15	10	020109	1	−3.9	0.045	2.6	532	ORI
	025934	10	25	025928	6	−7.2	0.150	8.7	723	ORI
	040428	19	15	040427	1	−3.7	0.015	0.9	572	ORI
	040500	11	8	040457	3	−3.1	0.094	5.4	569	SPO
	043449	18	7	043448	1	−3.0	0.009	0.5	539	ORI
	044350	9	8	044344	6	−5.0	0.250	14.5	505	ORI
	044402	19	13	044356	6	−3.4	0.303	17.7	387	ORI
*1				025210		−3.0	0.158	9.1	487	SPO
*2				045925		−2.9	0.103	5.9	453	ORI

4. The farther the distance, the weaker the intensity; the echoes could not be detectable farther than $D > 1000$ km.

   We can state such relation with another expression; the intensity of the echoes decreases with the distances from the sites ($D = R_1 + R_2$) (Figure 8d). When a meteor rushes into the atmosphere farther than 600 km from the sites, the intensity of the echo might be smaller than 10, that is, automatic counting level rejecting noises in usual HRO. Though we use remarkable echoes, that is, rather intense ones, it seems that the upper limit of the distances D might be no farther than 1000 km.

We cannot find remarkable echoes such as those produced by Orionids in the Geminid observations during 2018 December 13–15, except for a few sporadic meteors. We selected typical echoes of Geminids shown in Table 2. These echoes are from meteors near both sites, that is, short distance ($D = R_1 + R_2$) and, therefore, echoes are easily recognizable though M_a are not so bright.

It is unfortunate for us that typical Geminids are distributed within such narrow ranges in the distance and the absolute magnitude that we could not get useful information to realize the standard for collation. We therefore apply the tentative standard to Orionid and Geminid records hereafter.

4.2 The application of the standard

Figure 9 gives an example of the HRO recording in 2018 December 14, $05^{\rm h}10^{\rm m}$–$05^{\rm h}20^{\rm m}$ (JST=UTC+9). We can easily recognize the following 13 signals as meteor echoes (hhmmss: hour+minute+second):
hhmmss = 051026, **051252**, 051321, **051425**, 051429, 051533, 051640, 051658, 051753, 051818, 051834, 051842, **051927**

We can search video meteor records through SonotaCo net and find the following 11 meteors in the same period:
hhmmss = 051015, 051015, 051212, 051246, **051251**, 051314, **051425**, 051515, 051652, 051810, **051926**

We easily identify 3 meteors printed in bold above are observed by both HRO and video observations by applying the standards stated above. Table 3 gives the geometrical data of video meteors as shown in Figure 2. We realize the reason why only 3 meteors are recorded by HRO; IPs of the 3 simultaneously recorded meteors (bold numbers) are much smaller than other 8.

IP plays an important role in the collation, but it is only one factor for the research; it is very natural that the absolute magnitude and the distance from the origin are important factors. Other than IP, we applied the standard obtained from the remarkable echoes of Orionids to Orionids (2009 October 21, $22^{\rm h}00^{\rm m}$ to October 22, $05^{\rm h}00^{\rm m}$) and to Geminids (2018 December 14, $19^{\rm h}00^{\rm m}$ to December 15, $05^{\rm h}30^{\rm m}$).

Figures 10a and 10b show examples of the results; the distribution of the midpoints of Geminids (a) 2018 December 15, $04^{\rm h}00^{\rm m}$–$05^{\rm h}00^{\rm m}$ (JST=UTC+9), and Orionids (b) 2009 October 22, $04^{\rm h}00^{\rm m}$–$05^{\rm h}00^{\rm m}$ (JST). The collated meteors (filled circles) are distributed in the reasonable area, that is, the standards we used are proper to apply to different cases.

Table 2 – Typical Geminids' echoes. See Table 1 for the caption.

Date	HRO	I	$Dur.$	Video	Δt	M_a	IP	D
12/13	211234	25	6	211233	1	−0.8	0.062	278
12/14	051252	18	5	051251	1	−1.2	0.088	327
	052401	24	6	052359	2	0.0	0.034	312
	211235	24	6	211234	1	0.1	0.129	295
	212450	28	5	212450	0	0.0	0.137	283
	212835	18	4	212835	0	−1.3	0.077	347
	213431	17	8	213429	2	−1.7	0.326	236
	224218	24	5	224217	1	−0.4	0.083	356
	233525	16	7	233524	1	−3.6	−0.018	440
12/15	052955	23	6	052953	2	−2.6	0.062	312

Table 3 – Video meteors during 2018 December 14, $05^{\rm h}10^{\rm m}$–$05^{\rm h}20^{\rm m}$. M_a is absolute magnitude, x, y are the coordinates of the middle point of the meteor path centered at the halfway point of the emitter and the receiver, H_m is the height of the midpoint of the meteor path, a and b are the semi-axes of the ellipsoid (see Figure 2), IP is the inner product.

Time	M_a	x	y	H_m	a	b	IP
051015	−1.5	395	−174	87	444	439	−0.571
051015	−2.8	439	−64	84	457	452	−0.487
051212	−2.6	−6	−18	97	118	98	0.902
051246	−0.1	319	−94	90	351	344	−0.471
051251	−1.2	120	12	89	164	150	0.007
051314	0.1	306	−82	88	334	328	−0.383
051425	−0.8	157	81	91	208	197	0.032
051515	−2.6	−96	57	87	154	140	0.977
051652	−0.8	388	−62	90	408	403	−0.504
051810	−0.7	87	224	87	258	249	0.266
051926	−0.1	106	−54	89	161	147	−0.069

4.3 The differences between Orionids and Geminids

Though our standards proved to be effective, we find some differences between the results of Geminids and Orionids. Tables 4 and 5 show the summaries of the collation for comparison. We get 69 collated Geminids and 29 Orionids; the ratios to all video shower members are 7.4% and 5.7% respectively.

We can confirm the conjecture described in Section 3.3 (Comparison between Orionid and Geminid echoes). The intensity of Geminids seems to be higher than Orionids; the maximum intensity in the collated echoes, the first line of each statistic, and the median, the third line, both suggest Geminids give more vivid echoes than Orionids. The median of the duration, the third line, indicates Geminids could produce longer echoes, though Orionids exhibit long splendid echoes occasionally (the maximum in the first line).

The median of H_m (the height of the midpoint of the meteor path), the third line, indicates Orionids fly more than 15 km higher than Geminids do. This difference works very importantly in obstructing Orionid observations by HRO as shown in Section 6 (Orionids and the ceiling height).

HRO catches Orionids at a farther distance $D = R_1 + R_2$ than Geminids. Figure 11a shows the relation of the distance with the altitude of the radiant of collated meteors. It is clear that HRO records farther meteors, both Orionids and Geminids, according to the rise of the radiant as shown in Figure 2. It is, therefore, natural that the intensity of echoes decreases with the altitude (Figure 11b), because the distance increases with the altitude. We need then notice the concentration of Orionids' echoes in the high limits, that is, over 70 degrees. This partiality causes the difference between Orionids and Geminids with regard to the intensity and the distance (Table 4 and 5); Orionid echoes are few at lower radiant altitude.

We can exhibit the difference between echoes of Orionids and Geminids by comparing their figures also (Figure 12). Two sets of echoes each having similar character (M_a, D and IP, see Table 6) represent the differences between Orionids and Geminids in the intensity and the duration. Two Orionid echoes are shown at the left in each row and 6 Geminid echoes are to their right. Orionids give impressive echoes occasionally (Figure 12 the leftmost figure of the upper row) but express thin echoes often (Figure 12 the leftmost figure of the lower row). As the medium durations of Geminids' echoes are longer than Orionids' (Tables 4 and 5), echoes of Geminids in Figure 12 remain a few seconds: several pixels.

We already recognized that the difference in meteor rate shifts in Figure 4a and 4b and can add now signs of the different nature of Orionids and Geminids: the height of meteor trails, and intensity and duration of echoes. It is suggested that the difference in the height may be the cause of the puzzles. We will study where the differences come from in the next sections.

5 What class of echoes HRO catches: estimation of the electron line density from video observations

HRO cannot report the electron line density, because HRO intend to record meteor rates easily. Though it is necessary to accept many hypotheses to calculate the electron line density from optical meteor observations, the results can help us to understand the characteristics of radio meteors more widely. We estimate the mass of the meteoroid firstly and study the electron line density based on the classical physical theory of meteors ignoring the fragmentations, the thermal conduction, and the heat capacity of the meteoroid, etc.

Table 4 – The summary of the collation for Geminids; the total simultaneous meteors are 69 of 935 video Geminids in the searched period 2018 December 14, $19^{\rm h}00^{\rm m}$ to December 15, $05^{\rm h}30^{\rm m}$. The first line in each statistic shows the maximum values, the second line the minimum values and the third the median values. Last 3 lines give the statistics for not collated Geminids.

Geminids	Intensity	Duration	Δt	M_a	H_m	D	L	IP	Altitude
collated	34	14	7	1.3	137.3	842.8	56.3	0.915	87.9
	5	1	−1	−5.2	70.4	234.4	7.5	−0.229	27.9
	13	4	1	−2.2	86.4	385.9	22.5	0.041	61.8
all				2.3	184.8	1454.4	66.2	0.998	89.5
				−5.4	48.7	209.0	4.4	−0.839	14.7
				−1.3	87.7	476.7	17.0	0.332	70.5

Table 5 – The summary of the collation for Orionids; the total simultaneous meteors are 29 of 512 Orionids in the searched period 2009 October 21, $22^{\rm h}00^{\rm m}$ to October 22, $05^{\rm h}00^{\rm m}$. The first line in each statistic shows the maximum values, the second line the minimum values and the third the median values. Last 3 lines give the statistics for not collated Orionids.

Orionids	Intensity	Duration	Δt	M_a	H_m	D	L	IP	Altitude
collated	26	35	6	−0.4	108.4	956.5	72.6	0.506	73.5
	6	1	0	−7.2	99.5	250.6	8.9	−0.144	19.3
	9	2	2	−2.3	102.8	532.4	21.2	0.010	71.4
all	2.1	115.2	1273.9	91.4	0.998	73.5			
				−7.2	72.0	239.3	4.4	−0.630	10.4
				−1.3	104.2	543.3	15.8	0.527	67.3

5.1 The mass of the meteoroid

Öpik (1958) presents two formulae for the mass estimation: $\log m = 10.97 - 1.7 \log v - 0.4 M_a$ and $\log m = 10.02 - \log L - \log \tau - 3 \log v - 0.4 M_a$. m: mass of the meteoroid in grams, v: the velocity of the meteoroid in cm/s, M_a : the absolute magnitude of the meteor, L: the length of the meteor path in cm, τ: the luminous efficiency. Though the validity of the upper one is limited to $m < 1$ g, we use both formulae to estimate the meteoroid mass because it may be around 1 g. Öpik (1958) investigated the luminous efficiency in detail and showed a simple expression for the dustballs: $\tau = 2000/v$. But the following expression is usually applied: $\tau = kv$.

For example McKinley (1961) presented $k = 8.5 \times 10^{-5}$ of Whipple (1943) in his famous "Meteor Science and Engineering", but we use here $k = 5.25 \times 10^{-10}$ (in cgs) after Verniani (1965) in the following formulae.

Bronshten (1981) presents another expression for the meteoroid mass:

$$m = \frac{9}{2} \frac{H^* I}{\tau v^3 \cos z}$$

I: the luminous intensity in erg/s, z: the zenithal angle of the radiant (not radiant altitude), H^*: the scale height. Öpik (1958) gives the following formula for the transformation of the absolute magnitude of the meteor into the luminous intensity, $\log I = 9.72 - 0.4 M_a$. The scale height is expressed as follows, $H^* = \frac{RT}{Mg}$. R: universal gas constant ($R = 8.314$), T: absolute temperature at the height H, M: mean molecular weight at the height H, g: gravity acceleration at the height H. We can calculate g at any height easily. Though T and M change with the height H and vary with time, they can be treated as constant with meteor height according to the table A-1 of McKinley (1961), and we use $T = 199.3$, $M = 27.56$.

5.2 The electron line density

It is necessary to introduce the ionization efficiency β firstly to calculate the electron line density from the meteoroid mass assuming it is proportional to the kinetic power loss of the meteoroid like the luminous intensity. Many researchers have proposed many approximate formulae for the ionization efficiency, but Bron-

Table 6 – The details of echoes exhibited in Figure 12.

HRO	Intensity	Duration	Time	Δt	M_a	H_m	L	D	IP	Altitude	class	V_g
Figure 12 upper row												
012428	26	35	012428	0	−4.3	103	34.7	372	−0.012	52.1	ORI	67.5
232424	14	8	232424	0	−3.5	82	37.7	386	−0.041	64.9	GEM	32.0
235431	9	7	235429	2	−4.4	70	54.6	410	0.063	70.5	GEM	32.6
042145	5	3	042143	2	−4.0	81	8.6	403	0.088	60.8	GEM	31.2
Figure 12 lower row												
015340	9	1	015339	1	−1.0	107	11.8	376	0.013	57.6	ORI	66.0
224218	24	5	224217	1	−0.4	87	14.2	356	0.083	56.8	GEM	34.6
233427	13	5	233426	1	−1.3	89	17.2	391	0.024	66.8	GEM	31.1
043314	14	5	043312	2	−1.2	90	20.8	354	0.126	58.5	GEM	33.3

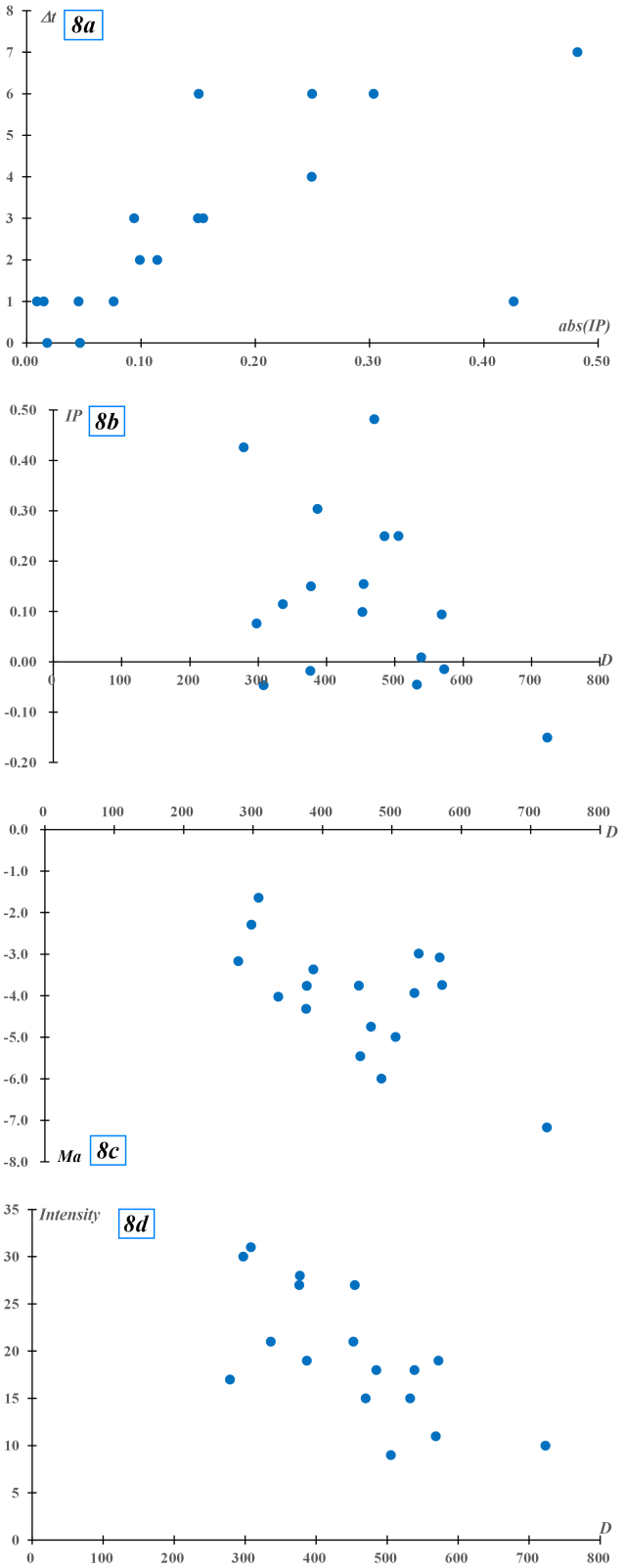

Figure 8 – a.) The absolute IP and the time lag Δt. b.) The distance $D = R_1 + R_2$ and IP. c.) The distance $D = R_1 + R_2$ and the absolute magnitude of the meteor M_a. d.) The distance $D = R_1 + R_2$ and the intensity of the echoes.

shten (1981) and Jones (1997) showed there is no simple formula which can express all types of meteoroids and their flight in the atmosphere. Bronshten (1981) showed widely different values of β based on different hypotheses for the meteoroid (Table 23 in his book), and Jones (1997) gave two different formulae; $\beta = 9.4 \times 10^{-6}(V - 10)^2 V^{0.8}$ for faint radio meteors ($V < 35$ km/s) and $\beta = 4.91 \times 10^{-6} V^{2.25}$ for visual meteors ($30 < V < 60$ km/s) both V in km/s. It is, therefore, necessary to realize that the following calculations show only rough estimation.

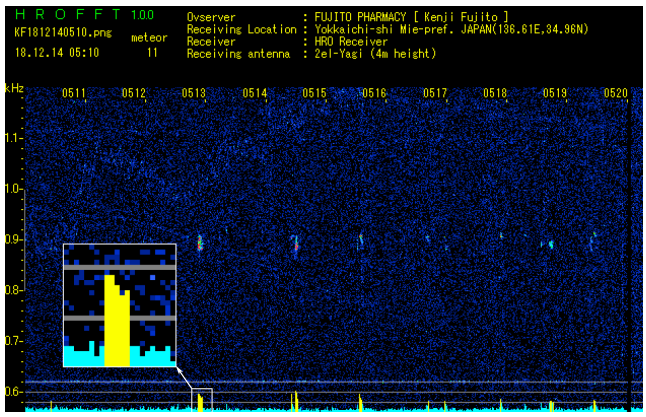

Figure 9 – An example of the HRO recording; 2018 December 14, 05^h10^m–05^h20^m (JST= UTC+9).

Bronshten (1981) presented the following formula to estimate the electron line density:

$$\alpha = \frac{4}{9}\frac{\beta m \cos z}{\mu H^*}$$

m: the average mass of a meteoroid atom 3.8×10^{-23} g according to Öpik (1958), β the ionization efficiency used here according to Verniani (1965): $\beta = 9.5 \times 10^{-29} v^4$. If we substitute the above Bronshten expression for m into his electron line density formula, we can get the following Verniani (1965) formula:

$$\frac{I}{\alpha} = \frac{\tau}{\beta} v^3 \frac{\mu}{2}$$

When we would not calculate the mass of the meteoroid, this formula might be useful.

We could mention two other formulae for calculating the electron line density without directly referring to the ionization efficiency. Verniani (1973) showed: $\alpha = 7.7 \times 10^{-10} m^{0.92} v^{3.91} \cos z$.

Belkovich (2006) presented this formula by using Tokhtasjev's ionization efficiency:

$$\alpha = 4.03 \times 10^{14} \frac{m(v - 8.15)^3}{H^*}$$

We estimated the electron line density of video meteors by the above mentioned methods. It should be stressed that we hypothesized the meteor phenomena in the atmosphere using simple physical theory of meteors and, therefore, the results might be only rough estimations.

5.3 The results

Table 7 shows the estimated mass of the meteoroids and the electron line density of Orionid and Geminid echoes listed Tables 1 and 3 respectively. We give two mass estimations by Öpik (1958) as described in the

Table 7 – The meteoroid mass and the electron line density estimated from video observations for Geminids and Orionids along with their hypothetical magnitude +4 meteors. Time is the same as Tables 1 and 3, IP is the inner product of the meteor path with the normal line of the ellipsoid, class is the IAU shower code, Ö/V are the electron line density by Verniani based on two mass estimations of Öpik. Some of m and α are given in exponential format: 4.1E+16 = 4.1×10^{16}.

Time	M_a	IP	class	V_g	m (g)			α (electron/m)			
					Öpik	Öpik	Bronshten	Ö/V	Ö/V	Bronshten	Belkovich
051251	−1.2	0.001	GEM	33.7	2.16	3.35	0.76	4.1E+16	6.1E+16	1.4E+14	8.7E+14
051425	−0.8	−0.032	GEM	33.7	1.55	1.94	0.55	3.0E+16	3.7E+16	1.0E+14	6.3E+14
051926	−0.1	−0.069	GEM	32.1	0.91	0.99	0.37	1.5E+16	1.6E+16	5.6E+13	3.4E+14
	+4			33.4	0.02	0.03	0.01	5.4E+14	7.8E+14	1.3E+12	7.1E+12
012428	−4.3	0.004	ORI	67.5	12.22	21.49	0.96	2.8E+18	4.7E+18	2.7E+15	1.4E+16
025928	−7.2	−0.144	ORI	67.7	168.90	361.51	10.32	4.0E+19	8.1E+19	3.7E+16	1.5E+17
044356	−3.4	0.279	ORI	67.4	5.11	6.90	0.31	1.6E+18	2.1E+18	1.1E+15	4.4E+15
	+4			65.4	0.01	0.01	4.3E−04	2.7E+15	3.3E+15	1.3E+12	5.4E+12

former section and one by Bronshten (1981). The electron line density estimations are four; two are by Verniani (1973) based on the two mass estimations of Öpik (1958); by Bronshten (1981); and by Belkovich (2006) using Bronshten's mass estimation also.

The mass estimations by Öpik are larger than others especially for Orionids, because he estimates luminous efficiency is inversely proportional to the meteoroid velocity. It seems to be proper to hypothesize it is proportional to the velocity and Bronshten's estimation seems to be better.

The estimations of the electron line density differ by more than hundreds. This is caused by the difference in ionization efficiency estimations used by them, because the difference in the estimated mass does not affect the electron line density estimation much. We can recognize the simultaneous meteors make overdense echoes, though the estimation differs widely.

It seems natural that the fainter meteors generate less dense echoes and, therefore, the electron density of the 4th magnitude meteors shown in Table 7 on the transitional electron line density; McKinley (1961) found it as $\alpha = 2.4 \times 10^{14}$ electrons/m and also referred to a slightly different $\alpha = 1.1 \times 10^{14}$ electrons/m. The estimation by Öpik-Verniani (Ö/V) suggests the 4th magnitude meteors produce overdense echoes, but those of Bronshten and Belkovich underdense. It is possible to consider fainter than 4th magnitude meteors might produce underdense echoes.

It is interesting to compare data of echoes simultaneously observed by video with those not observed by video. Figure 13 shows the echoes of Geminids listed in Table 7 and other echoes of the same observation period (see Table 3 also). The left three echoes observed simultaneously represent peculiar characteristics of overdense echoes, but the other two echoes seem to be underdense echoes which last only 1 second.

Figure 14 represents the similar comparison for Orionids; the left one is 025928 of Table 7 and the other four echoes are recorded in the same observation period: 2009 October 22, 02^h50^m–03^h00^m (JST=UTC+9). The echo 025928 is produced by a bolide ($M_a = -7.2$, see Table 7) and exhibits a characteristic appearance of an overdense echo, though it entered the atmosphere far from the stations (D = 723 km, see Table 1) and its echo is faint. This echo seems to be a representative figure of an overdense echo observed from a far point. The other four echoes look like two Geminid echoes of Figure 13, and they are thought to be underdense ones.

Such possible underdense echoes cannot be caught by video observations because almost all meteors recorded by SonotaCo net are brighter than 2nd magnitude (Figure 6c). It is suggested HRO can perceive underdense echoes, fainter than 4th magnitude, which arise along the surface of the ellipsoid having focuses as the transmitter and the receiver. We can estimate HRO can record meteors not fainter than 6th magnitude, as visual observers can, because echoes having no video observations in Figures 13 and 14, possible underdense echoes, are slightly above the HRO detection level.

6 Orionids and the ceiling height

We have pointed out that HRO records smaller ratios of Orionids to video rates than Geminids when Orionids' radiant is not high enough (Figure 7). We can infer the cause comes from the difference between Orionids and Geminids in their midpoint of the height (see Section 4.3. The difference between Orionids and Geminids). Figure 15a shows the moving mean of the midpoint height in 5 time-sequence bins for Orionids against their radiant altitude; it is natural that meteors radiate higher in the atmosphere when they fly into the atmosphere slanting low as seen in case of Geminids also (Figure 15b). But it seems the difference of about 15 km in the height of the midpoint (see also Table 4 and 5) plays a very important role in the smaller echo ratio to video in Orionids than Geminids.

McKinley (1961) wrote we cannot receive meteor echoes when the power loss in decibels given in the following formula becomes higher than 40 dB.

$$\text{Loss in dB} = 970\frac{R_0^{1/2}D}{\lambda^{3/2}V} + 343(\frac{r_0}{\lambda})^2$$

Where R_0 is the distance to the minimum range point in meters, λ radio wavelength in meters, V meteoroid velocity in m/s. D is the diffusion coefficient and is summarized for the region between $80 < H < 110$ km by the relation $\log D = 0.067H - 5.6$. r_0 is the initial radius of the meteor path in meters and could be ex-

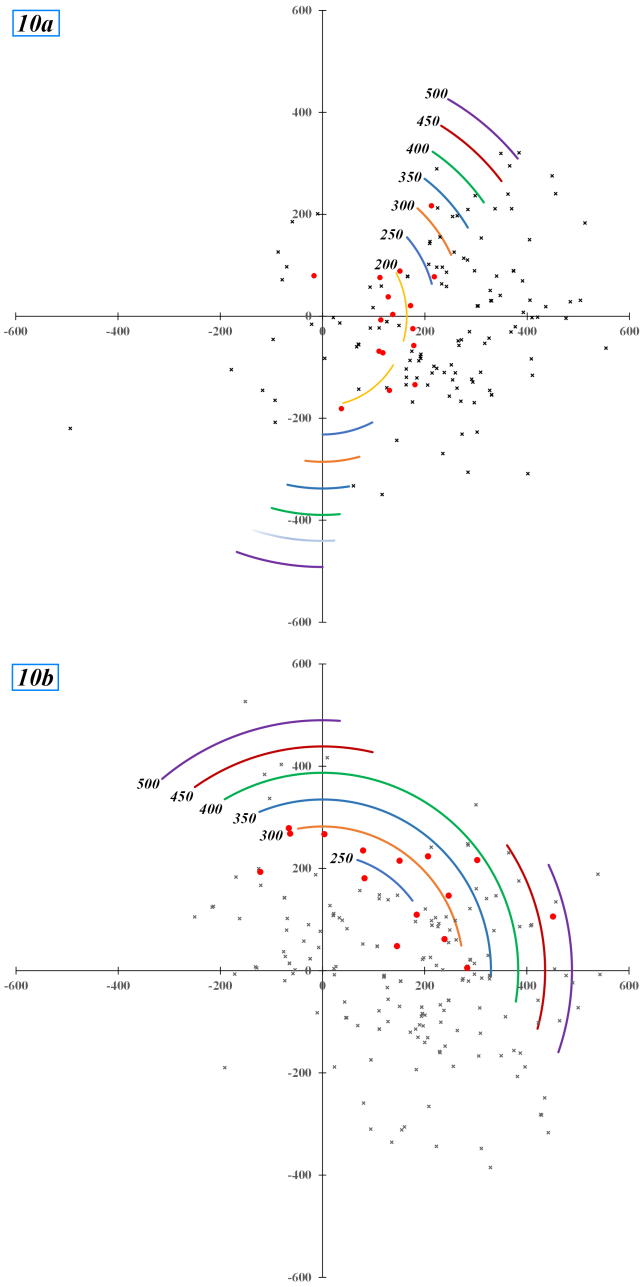

Figure 10 – a.) Collated Geminid meteors (filled circles) with others (crosses) in the period of 2018 December 15, $04^{h}00^{m}$–$05^{h}00^{m}$ (JST=UTC+9). y-axis runs through the emitter–receiver line and the arcs show the $IP < 0.1$ area with the distance from the center in km. b.) Collated Orionid meteors (filled circles) with others (crosses) in the period of 2009 October 22, $04^{h}00^{m}$–$05^{h}00^{m}$ (JST=UTC+9). y-axis runs through the emitter–receiver line and the arcs show the $IP < 0.1$ area with the distance from the center in km.

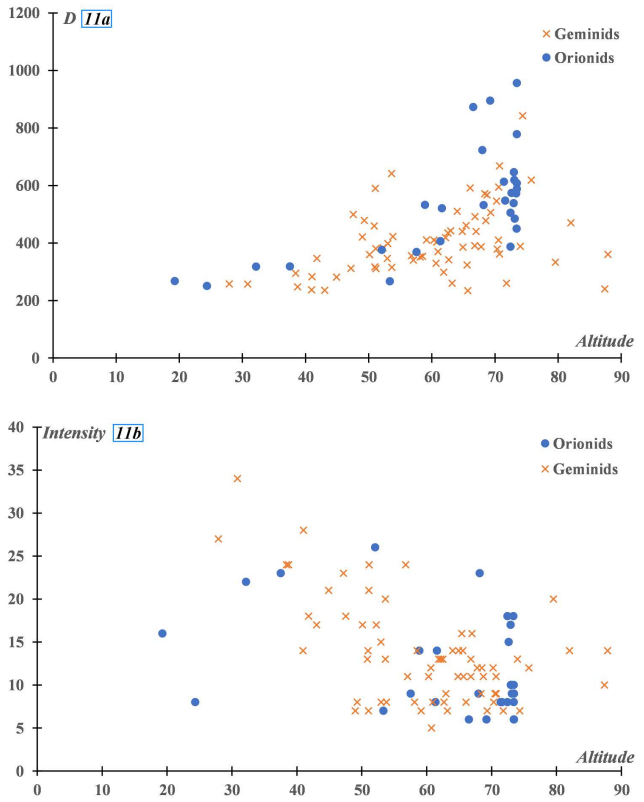

Figure 11 – a.) The relation of the distance ($D = R_1 + R_2$) with the altitude. b.) The relation of the intensity with the altitude.

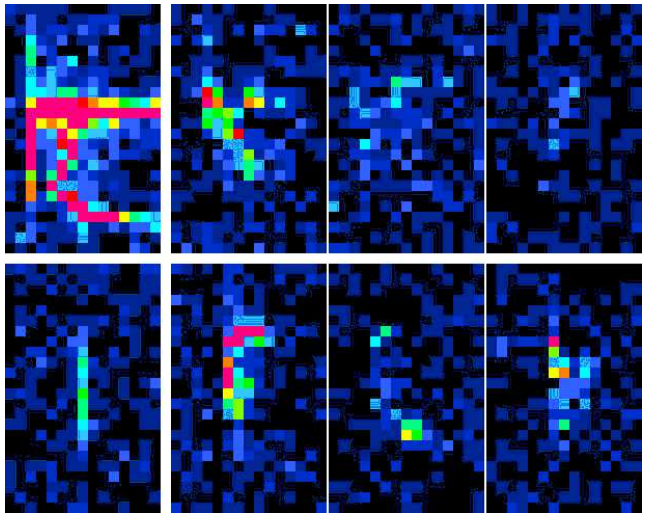

Figure 12 – The comparison of echoes of Orionids and Geminids having similar character: M_a, D and IP. Each one pixel corresponds to one second. The upper row: 012428 (ORI), 232424 (GEM), 235429 (GEM) and 042143 (GEM) left to right. The lower row: 015339 (ORI), 224217 (GEM), 233426 (GEM) and 043312 (GEM)left to right.

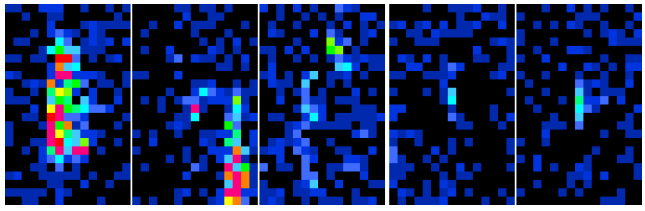

Figure 13 – Echoes recorded in the period of December 14, $05^{h}10^{m}$–$05^{h}20^{m}$ (JST). Left three are observed by video simultaneously; left to right 051251, 051425 (featured in the center), 051926. Right two figures are 051321 (left) and 051834 (right). See details Table 7.

pressed for $75 < H < 120$ km by the following relation: $\log r_0 = 0.075H - 7.9$.

He indicates 'It should be emphasized that the ceiling defined here applies to underdense-type echoes' but comments also 'Under certain conditions an overdense trail can yield an underdense-type echo.' We calculated the height of echo power attenuation 40 dB as a function of meteoroid velocity; we adopted $\lambda = 6$ m, that is, in the case of 50 MHz used in HRO ordinarily, adding a case of 80 MHz for FM radio. Figure 16 gives the

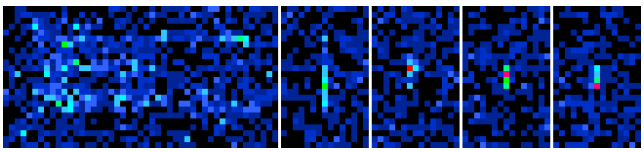

Figure 14 – Echoes recorded in the period of October 22, 02^h50^m–03^h00^m (JST) . Only 025928 is observed by video (left) and other 4 echoes (right) are not recorded by video. They are recorded at 025312, 025340, 025832, 025906, respectively.

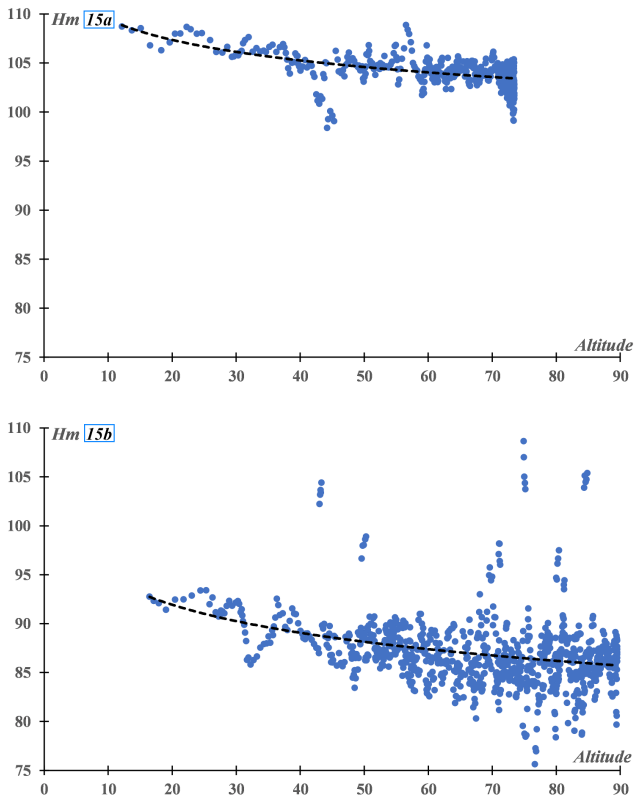

Figure 15 – The moving mean of the midpoint height in 5 time-sequence bins against their radiant altitude, the broken line indicating the logarithmic best fit. a: Orionids, b: Geminids.

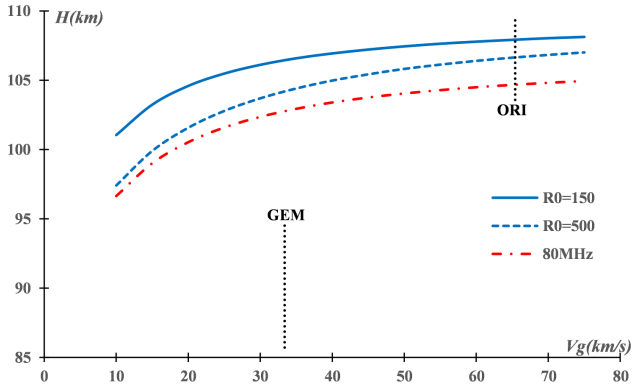

Figure 16 – The height of echo power attenuation 40 dB as a function of meteoroid velocity; we adopted $\lambda = 6$ m, that is, in case of 50 MHz used in HRO ordinarily, adding a case of 80 MHz for FM radio. $R_0 = 150$ km and $R_0 = 500$ km are for 50 MHz and the 80 MHz case has $R_0 = 150$ km. The dotted lines indicate the probable range estimated from the logarithmic best fit of the relation of the height with the altitude of the radiant shown in Figure 15.

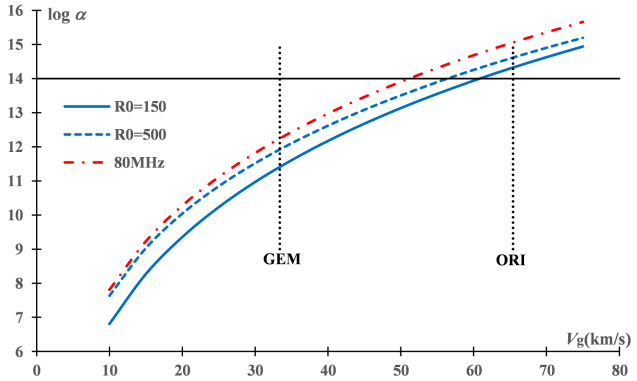

Figure 17 – The electron line density of attenuation 40 dB as a function of meteoroid velocity; we adopted $\lambda = 6$ m, that is, in the case of 50 MHz used in HRO ordinarily, adding a case of 80 MHz for FM radio. $R_0 = 150$ km and $R_0 = 500$ km are for 50 MHz and the 80 MHz case has $R_0 = 150$ km. The dotted lines show the mean geocentric velocity of the showers.

contour of the function. We selected $R_0 = 150$ km for the minimum distance and $R_0 = 500$ km for the maximum condition of HRO observations (see Table 4 and 5) in the case of 50 MHz; $R_0 = 150$ km for 80 MHz. The ranges above each line express the height where the loss in decibels becomes larger than 40 dB and we cannot receive meteor echoes, this is the height ceiling.

It is clear the ceiling height becomes lower when we use shorter wavelength; two lines of 50 MHz (solid and broken line) are above the line of 80 MHz (dashed-dotted line). This is the reason why professional meteor radars operate around 30 MHz.

We can realize the ceiling height becomes higher with the meteor velocity and, therefore, it might be suggested we can hardly record echoes of slower meteors. This is not so because slower meteors start to radiate at a lower height than faster meteors; the estimated midpoint of Geminids is located lower than Orionids and sufficiently under the ceiling height (Figure 16). We cannot receive echoes of fast meteors, such as Orionids, satisfactorily but can record ones of moderate speed meteors, Geminids: we observe still slower meteors with difficulty by HRO because of their insufficient electron line density (see the formulae in the former section).

It is very interesting the estimated midpoint of Orionids extends over all three lines (the dotted line of Figure 16). The midpoint of meteor paths changes with the altitude of the radiant as we showed in Figure 15a and 15b; the top of the dotted line indicates the estimated midpoint for the radiant altitude 10 degrees and the bottom 70 degrees (Figure 16). This is the reason why we observe rather few Orionid echoes when its radiant lies low and the echo numbers increases with the radiant altitude.

Figure 17 gives another aspect for the height ceiling; all three lines show the electron line density defined by the loss in the echo power attenuation 40 dB and we cannot receive echoes from the area under the line. We expect we can catch almost all Geminids echoes ($\log \alpha > 12$) but not so Orionid echoes.

Table 8 – Electron line density and the estimated radio magnitude for Geminids and for Orionids.

$\log\alpha$	18	17	16	15	14	13		Vg
M_r	−5.4	−2.5	0.4	3.3	6.2	9.1	GEM	33.4
	−4.5	−2.1	0.3	2.8	5.2	7.6	ORI	65.4

McKinley (1961) estimates the relation of the radio magnitude M_r with the electron line density α and the meteor velocity as follows:

$$M_r = \frac{71 - 4.4\log\alpha}{\log V}$$

We can calculate the estimated radio magnitude for Geminids and Orionids against the electron line density as shown in Table 8; if we adopt the transitional electron line density between overdense and underdense echoes as $\alpha = 2.4 \times 10^{14}$, M_r values are magnitude +5.1 and +4.3 for Geminids and Orionids, respectively.

We realize HRO can detect every Geminid echo appeared in the proper range and above the perception limit of our system which is estimated as 5$^{\text{th}}$ to 6$^{\text{th}}$ magnitude as shown in the former section. On the other hand, all three lines suggest we can recognize only overdense echoes for Orionids, though Figure 16 indicates we can receive underdense Orionid echoes when the radiant altitude is high enough.

The electron line density α might be in proportion to $\cos z$ according to the formulae of Bronshten or Verniani and, therefore, α could be larger when the radiant is low than around the culmination. It could be the reason why HRO–video ratios of meteor rates of Geminids at low altitude are higher than those of around the culmination (Figure 7). If the height ceiling would not affect on the observations, Orionids echo rates might be higher than the observed one and similar to Geminids shown in Figure 7.

7 Discussion: what range of meteors can HRO recognize?

The sporadic E layer and neighboring noise significantly hinder HRO and we know HRO has some other difficulties explained above. We can get what kind of knowledge from HRO and what are its properties?

We know numbers of echoes from meteors vary with time, the minimum in evening and the maximum in morning every day as optical observations show, though the ratio of the maximum to minimum is larger in video observations than HRO. Yearly changes could show more clearly the specific characteristics of HRO against other techniques.

Figure 18a–c express the comparisons of meteor rates by four different observational techniques year-round. They are normalized to average meteor rates of 100 and drawn on the graph of HRO for comparison.
HRO (Fujito, this paper): 2018 July 17 to 2021 May 31.
CMOR (Canadian Meteor Observations of Radar): 2017, $\lambda_\odot = 119$ to 2021, $\lambda_\odot = 42$.
Olivier (Visual, Olivier, 1960): 1901–1958.
Video (Sonota Co net, SonotaCo, 2009): 2007–2018.

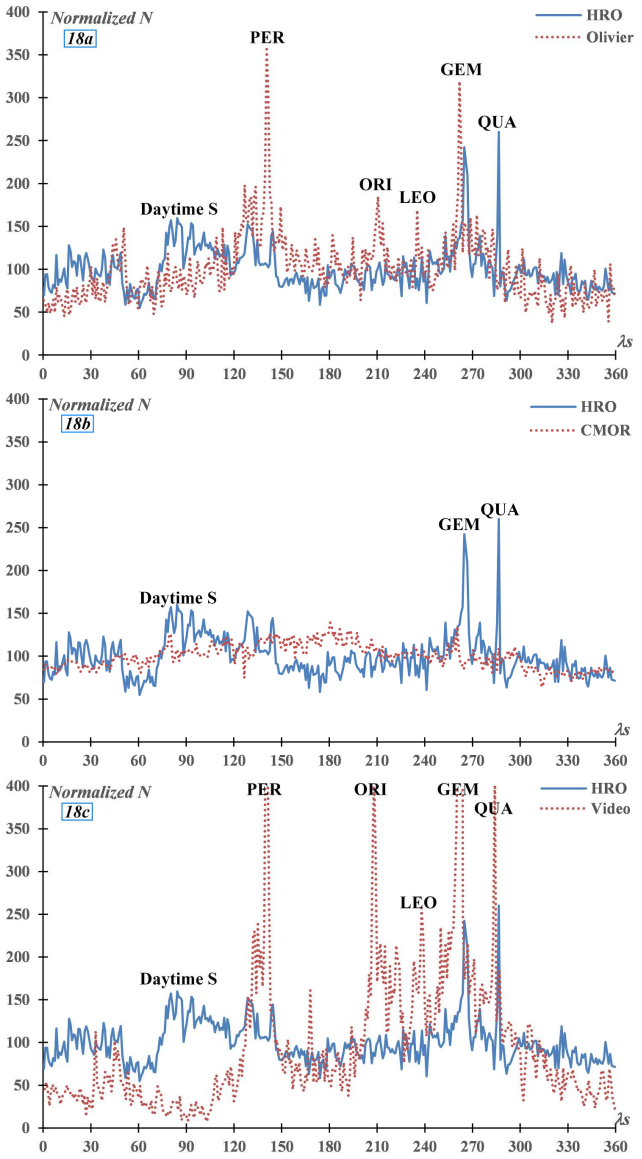

Figure 18 – a.) The comparison of HRO with Olivier (visual) in the normalized number; each yearly averages is 100. b.) The comparison of HRO with CMOR in the normalized number; each yearly averages is 100. c.) The comparison of HRO with Video observations in the normalized number; each yearly averages is 100.

Figure 18a shows the comparison of HRO rates with visual observations. Olivier (1960) published a large table of 'Catalog of Hourly Meteor Rates' covering 1901–58 visual observations mainly from AMS. He compensated raw recorded meteor numbers by his unique method to the listed hourly meteor rates because naked eye observations are hindered by many conditions: cloud, moon, transparency of the sky and so on. We can easily find the yearly variations in visual rates are similar to HRO. Visual data represents major shower activity as in the case of HRO: Perseids, Orionids and Geminids. Quadrantids are absent in visual observations because of bad weather conditions in January for observers in USA and Europe. HRO shows clear Geminid and Quadrantid activities, but Perseids and Orionids are unclear, though daytime showers form a plateau in June (around $\lambda_\odot = 80$). Meteor showers of higher

velocity, such as Orionids, cannot be recorded fully by HRO because of the height ceiling effects.

Figure 18b shows the representative radar observations as a contrast with HRO. CMOR gives Norb as the number of daily recorded meteor orbits. CMOR stops completely for several days or sometimes records a smaller number than the full daily number because it needs some cooling time and is affected by the weather. We exclude such unusual records and show the mean value of records. Yearly variations in radar rates is somewhat different from HRO; CMOR rates have a rather simple pattern presenting one moderate peak in autumn. We cannot find clear traces of major showers such as Perseids and Orionids in CMOR. It is clear that ordinary radar observations of meteors are affected by the height ceiling more intensely.

Figure 18c shows the contrast resulting from comparison with video observations. We can use video data of SonotaCo net in the full period 2007 to 2018; we need 12 years to completely catch meteor shower activity because of 3 years of the moon's cycle and 4 years of the alteration in position of the Earth on its orbit. Video rates create sharp peaks of major showers also: Perseids, Orionids, Geminids and Quadrantids. Video observations in Japan are hindered much by two rainy seasons around $\lambda_\odot = 90$ and $\lambda_\odot = 180$ and are lower around those times. Yearly variations of video rates might resemble HRO if we consider the weather influences, though video peaks of major showers are very sharp. It is necessary to stress that video meteors are mostly $M_a < 0$ (Figure 6c) and showers rich in bright meteors are picked out preferentially.

It is suggested that HRO records meteors in a similar range as visual ones, in other words, HRO could not detect meteors as faint as CMOR can. HRO misses both slower and faster meteors which visual observers can catch, because the electron line density of slower meteors is smaller than faster ones and faster meteors are blocked by the height ceiling. We need to compensate raw visual data to get ZHRs of meteor showers; we are hindered by weather, moonlight, obstruction of the view and so on. We could compensate unique influences in radio observations as with visual data handling, HRO can give good profiles of meteor activities.

Optical observations including video cannot record daytime activities naturally and much hindered by sky circumstances. Video results depend on brighter meteors than visual and radio ones and are unique to the latter; video observations can perceive faster, brighter, and scarce activities. We should realize that every observation technique gives unique results.

Acknowledgements

We owed much to voluntary transmissions of the late Mr. Kimio Maegawa for SABAE and Fukui Prefectural University amateur meteor radio observation club for FUKUI. We would like to express our sincere thanks to them.

References

Belkovich O. I. (2006). "The physics of meteoroid ablation and the formation of ionized meteor trails". In Verbeeck C. and Wislez J.-M., editors, *Proceedings of the Radio Meteor School*. pages 21–26.

Bronshten V. A. (1983). *Physics of Meteoric Phenomena*. Reidel, Dordrecht. (originally published in Russian 1981).

CMOR, The Canadian Meteor Orbit Radar (CMOR) (2022). `https://fireballs.ndc.nasa.gov/cmor-radiants/earth.html` .

Jones W. (1997). "Theoretical and observational determinations of the ionization coefficient of meteors". *Mon. Not. R. Astron. Soc.*, **288:4**, 995–1003.

Koseki M. (2015). "What do we see as ANT, Apex and Toroidal sources? - What meteors are, where meteors came from, where meteoroids are going". *WGN, Journal of the International Meteor Organization*, **43:5**, 127–146.

McKinley D. W. R. (1961). *Meteor Science and Engineering.* McGraw-Hill, New York.

Ogawa H. (2022). "The international project for radio meteor observations". `https://www.iprmo.org/` .

Olivier C. P. (1960). "Catalog of Hourly Meteor Rates". *Smithsonian Contributions to Astrophysics*, **4**, 1–14.

Öpik E. J. (1958). *Physics of Meteor Flight in the Atmosphere.* Interscience, New York.

SonotaCo (2009). "A meteor shower catalog based on video observations in 2007-2008". *WGN, Journal of the International Meteor Organization*, **37:2**, 55–62. See also "SonotaCo Network Simultaneously Observed Meteor Data Sets", http://sonotaco.jp/doc/SNM/ .

Verniani F. (1965). "On the Luminous Efficiency of Meteors". *Smithsonian Contributions to Astrophysics*, **8**, 141–172.

Verniani F. (1973). "An Analysis of the Physical Parameters of 5759 Faint Radio Meteors". *J. Geophys. Res.*, **78:35**, 8429–8462.

Whipple F. L. (1943). "Meteors and the Earth's Upper Atmosphere". *Reviews of Modern Physics*, **15:4**, 246–264.

Handling Editor: Javor Kac

May 2022 – an exciting meteor month

Jürgen Rendtel[1]

Meteor observers had an exciting month of May in 2022. The annual return of the Eta Aquariids (031 ETA) yielded a broad peak ZHR of 40–tc50 lasting for more than 4 days, decreasing only on May 8. The Eta-Lyrid (145 ELY) ZHR reached the typical level of 3–4. Data close to the possible activity from the minor planet (461 852) 2006 GY_2 on May 15 revealed no peculiar rates. This also holds for the Camelopardalids (451 CAM) where rate enhancements were possible on May 25 according to model calculations. On May 31, the Earth encountered the meteoroids released from comet 73P/Schwassmann-Wachmann 3.

Received 2022 June 21

1 Introduction

The eta-Aquariids (031 ETA) related to comet 1P/Halley are the best known and most active annual meteor source in May. Weaker activity is expected from the eta-Lyrids (145 ELY) associated with comet C/1983 H1 (IRAS-Araki-Alcock) and from the continuously active Antihelion Source with its centre in Scorpius – Sagittarius.

For 2022, the IMO Meteor Shower Calendar listed three more (possible) meteor sources worth to check (Rendtel, 2021). The first two events are based on calculations by Jeremie Vaubaillon: on May 15, there was a chance that the Earth encountered meteoroids released from the minor planet (461 852) 2006 GY_2. On May 25, the Camelopardalids (451 CAM) of comet 109P/LINEAR were due. Finally, on May 31, the tau-Herculids (061 TAH) of comet 73P/Schwassmann-Wachmann 3 were expected.

This is a brief summary of the activity found from each of the cometary sources in May 2022. As an aside: this month had two New Moons.

2 η-Aquariids (031 ETA)

This is a strong and reliable meteor shower mainly for the southern hemisphere with a broad maximum on May 5. In 2022, the conditions for optical observations were perfect. The preliminary profiles of the visual ZHR and video meteor flux density are shown in Figures 1 and 2, respectively. The 2022 profile has rather little gaps which usually is the case due to the uneven geographical distribution of the observers in the southern hemisphere.

The profiles are very close to the average and show a ZHR exceeding 30 between $\lambda_\odot = 43°$ and 48°; the highest values reach a level of 50 with no specific structures. One surprising feature is the extension of the ZHR (and respective flux density) level of about 50 into May 8. Usually, the rate decreases in the course of May 7. Since the ETA are used for several calibrations of the video data (e.g. the zenith correction, collecting area), the close match of the ZHR (see right scale in Figure 2) underlines the reliability of the two independent data sets.

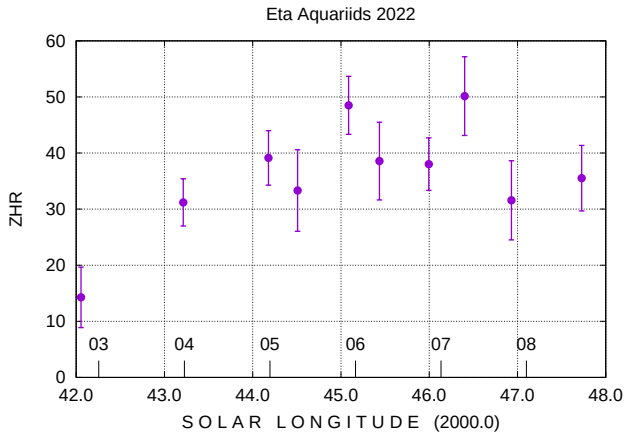

Figure 1 – Visual ZHR of the 2022 Eta Aquariid maximum period, calculated with a constant $r = 2.30$. The corresponding dates are given in the diagram and refer to 0^h UT.

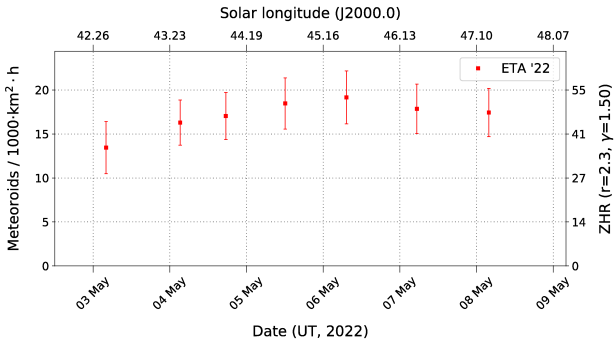

Figure 2 – Video flux density of the 2022 Eta Aquariid maximum period, calculated with a constant $r = 2.30$, using the preliminary data as provided by `https://meteorflux.org/` (accessed 2022 June 21).

3 η-Lyrids (145 ELY)

Observations of this minor shower are mainly possible from the northern hemisphere, where the duration of the dark night is already quite short. The rather low expected activity does not attract a lot of observers, hence the sample remains small and we can just state that the ZHR reached the known level of about 3–4 around May 10.

4 Meteors of (461 852) 2006 GY_2

The predicted encounter time was on May 15, close to 10^h20^m UT ($\lambda_\odot = 54\overset{\circ}{.}28$) according to calculations

[1]International Meteor Organization, Eschenweg 16, 14476 Potsdam, Germany. Email: `jrendtel@web.de`

IMO bibcode WGN-503–4-rendtel-may2022showers
NASA-ADS bibcode 2022JIMO...50...89R

Table 1 – Visual observations close to the calculated encounter of meteoroids from the minor planet (461 852) 2006 GY_2 stored in the VMDB in the night 2022 May 14/15 (i.e. the UT times refer to May 14 and 15, respectively). T_{eff} is the interval length, c_F the field correction, LM the limiting magnitude and HER the number of meteors associated with the given radiant. SPO and TOT are the numbers of sporadic meteors seen and the total number for comparison.

Period (UT)	$\lambda_\odot$ [°] start/end	T_{eff} hours	c_F	LM	HER	SPO	TOT	Observer and location
2355–0045	53.86	0.83	1.00	5.98	0	2	4	Jürgen Rendtel
0045–0135	53.93	0.83	1.00	6.04	0	5	6	Germany (52.°5 N; 12.°9 E)
0200–0240	53.94	0.67	1.00	5.00	0	2	5	Tim Cooper
0252–0338	54.01	0.77	1.00	5.20	0	0	0	South Africa (26.°09 S; 28.°32 E)
0920–1020	54.24	1.00	1.11	4.55	0	2	2	Robert Lunsford
1020–1120	54.32	1.00	1.00	5.09	1	1	2	USA (32.°86 N; 116.°86 W)

of Vaibaillon provided in Rendtel (2021). Unfortunately, this was just a day before the Full Moon (with a lunar eclipse on May 16) and the enthusiasm to observe visually in moonlit skies is generally small. The few reports in the vicinity of the predicted encounter time do not give signs of activity from the radiant at $\alpha = 248°$, $\delta = +46°$ which is just 3° east of the star τ Herculis. (Hence a possible shower should be called tau-Herculids while the 061 TAH radiate from Bootes – see below.) The calculated velocity of the meteoroids was 36 km/s. Vaubaillon pointed out that the density of asteroidal streams is difficult to estimate.

Only three reports in the VMDB explicitely mention that the observer checked for possible meteors from this source (Table 1; possible meteors associated with the radiant labelled as HER). So the visual data has no clue about an activity. Other reports are not known as well.

The periods covered by the available reports starts at $\lambda_\odot = 53.°86$ and ends at $\lambda_\odot = 54.°32$. Some activity was detected in radio forward scatter data (Ogawa & Sugimoto, 2022a) between 54.°325 and 54.°365 (May 15, 11^h30^m – 12^h30^m UT). That is just after the last period in our list so that the single meteor seen by Robert Lunsford may just be the start of this brief activity.

5 Camelopardalids (451 CAM)

Activity of this shower was predicted and observed on 2014 May 24 between 07^h30^m and 08^h00^m UT ($\lambda_\odot = 62.°87 - 62.°89$) with a ZHR of 10–15 (Jenniskens, 2014) from a radiant at $\alpha = 120°$, $\delta = +78°$ with a velocity of $V_g = 15$ km/s. This was caused by dust ejected from the parent comet in the 18th, 19th and 20th centuries. Another encounter was calculated by Vaubaillon (details given in Rendtel, 2021) to occur on 2022 May 25 near 08^h UT ($\lambda_\odot = 63.°8$). The modelling sugested that the densest part is not to be passed but trails of 1903 and 1909 with lower density are crossed. The expected radiant position was essentially the same as during the 2014 activity.

Like in the case described above, the number of visual reports for the Camelopardalids was also too small for a conclusion about the shower activity. It seems that there may have been a low rate before the calculated encounter time, but the sample is not sufficient. Perhaps observers already prepared their tau-Herculid campaigns a few days later.

Radio forward scatter data (Ogawa & Sugimoto, 2022b) indeed show some CAM activity between $\lambda_\odot = 63.°428$ (May 24, 22^h30^m UT) and $\lambda_\odot = 63.°828$ (May 25, 08^h30^m UT). This includes all the three visual sessions. The estimated average visual ZHR for the periods between 63.4 and 63.5 degrees was about 2 (radiant elevation 50 to 40 degrees); during the late intervals in Table 2 the radiant was between 30 and 25 degrees high). So the few possible shower meteors occurred rather around $\lambda_\odot = 63.°4$ which is at the begin of the radio rate enhancement.

6 τ-Herculids

The name of this shower is misleading and is based on the theoretical radiant calculated for the 1930 ap-

Table 2 – Visual observations close to the calculated maximum of the Camelopardalids (451 CAM) stored in the VMDB for the night 2022 May 24/25 (i.e. the UT times refer to May 24 and 25, respectively). T_{eff} is the interval length, c_F the field correction, LM the limiting magnitude and CAM, SPO and TOT are the number of meteors associated with either source. Sessions are sorted by start their time.

Period (UT)	$\lambda_\odot$ [°] start/end	T_{eff} hours	c_F	LM	CAM	SPO	TOT	Observer and location
2130–2230	63.39	1.00	1.00	6.63	1	6	10	Ina Rendtel
2230–2330		1.00	1.00	6.63	1	7	10	Germany (52.°45 N; 12.°92 E)
2330–0030	63.51	1.00	1.00	6.63	0	7	10	
2135–2240	63.39	1.08	1.00	6.32	2	5	9	Jürgen Rendtel
2240–2345		1.08	1.00	6.35	2	5	9	Germany (52.°5 N; 12.°9 E)
2345–0050	63.52	1.08	1.00	6.28	0	4	8	
0700–0800	63.77	1.00	1.00	5.35	0	2	2	Robert Lunsford
0800–0900	63.85	1.00	1.00	5.51	0	1	1	USA (32.°86 N; 116.°86 W)

proach. The background is described in detail in (Rao, 2021), including the doubtful activity on that occasion. When a successive breakup of the parent comet 73P/Schwassmann-Wachmann 3 was observed from end 1995 onwards, it soon became clear that there will be a close approach of the Earth to the fresh debris on 2022 May 31 (Lüthen, Arlt and Jäger, 2001). The (modern) radiant at $\alpha = 209°$, $\delta = +28°$ is rather close to the +4.9 mag star 12 Bootis, about 8° north of Arcturus, hence a designation including Bootes would be more appropriate.

Several model calculations have been published including dust of the 1995 trail and before. The respective results for the 1995 dust encounter in 2022 were on May 31 near 05^h UT. Additionally there may be activity from dust released at the end of the 19th century mainly before the 1995 dust (Wiegert et al., 2005). The entire analysis of the 2022 return will be presented in numerous papers. At this point we just have a look at the general shape of the ZHR profile which confirms the main peak shortly after 05^h UT as well as an earlier maximum close to May 30, 22^h UT which is weaker and much less pronounced. It may be associated with the meteoroids of the 1892 and 1897 dust from SW3.

Details of the TAH-Activity are subject of several papers in this issue of WGN.

References

Jenniskens P. (2014). "Camelopardalids (IAU#451) from comet 209P/LINEAR". *WGN, Journal of the IMO*, **42:3**, 98–105.

Lüthen H., Arlt R., and Jäger M. (2001). "The Disintegrating Comet 73P/Schwassmann-Wachmann 3 and Its Meteors". *WGN, Journal of the IMO*, **29**, 15–28.

Ogawa H. and Sugimoto H. (2022a). "Meteor activity related to 2006GY2 by worldwide radio meteor observations". *eMeteorNews*, **7**, 244–245.

Ogawa H. and Sugimoto H. (2022b). "Meteor activity related to 209P/LINEAR by worldwide radio meteor observations". *eMeteorNews*, **7**, 242–243.

Rao J. (2021). "Will Comet 73P/Schwassman-Wachmann 3 produce a meteor outburst in 2022?". *WGN, Journal of the IMO*, **49:1**, 3–14.

Rendtel J., editor (2021). *2022 Meteor Shower Calendar*. International Meteor Organization. IMO_INFO 3-21.

Wiegert P. A., Brown P. G., Vaubaillon J., and Schijns H. (2005). "The τ Herculid meteor shower and Comet 73P/Schwassmann-Wachmann 3". *MNRAS*, **361:2**, 638–644.

Handling Editor: Javor Kac
This paper has been typeset from a LaTeX file prepared by the author.

Tau Herculids

Tau Herculids 2022: Rate, number density, population index and geometrical effects from visual data

Jürgen Rendtel[1,2] *and Rainer Arlt*[1]

We analysed visual observation data of the Tau Herculids collected between 2022 May 28 and June 1. The population index r is 2.4 for entire sample. For the pre-peak period we find $r = 2.57 \pm 0.23$, the peak period yields $r = 2.38 \pm 0.06$. The ZHR maximum of the 1995 ejecta from comet 73P/Schwassmann-Wachnann3 (SW3) is found at $\lambda_\odot = 69\overset{\circ}{.}450$, i.e. May 31, 05^h04^m UT (±5 min) with a ZHR $= 55 \pm 7$, corresponding with a spatial number density ND $\approx 380 \times 10^{-9}\mathrm{km}^{-3}$ for meteoroids larger than 10 mg. An earlier maximum occurred at $\lambda_\odot = 69\overset{\circ}{.}207$, i.e. May 30, centred at 23^h UT with a ZHR $= 18 \pm 3$ and is tentatively associated with SW3-ejecta from 1892. Effects of the radiant shift due to the large zenith attraction of about 10° for the radiant close to the horizon are discussed.

Received 2022 July 15

1 Introduction

The encounter with the fresh debris of comet 73P/Schwassmann-Wachmann 3 (short SW3) on 2022 May 31 (described in detail e.g. in Rao, 2021) caused many observational efforts worldwide to observe the event under favourable circumstances. The very first calculations including the precise prediction of the encounter time was published by Lüthen et al. (2001). The first as well as later predictions of the major peak due to meteoroids released from SW3 after the breakup in 1995 agreed very well in their timing. A summary of recent predictions is given e.g. in the IMO 2022 Meteor Shower Calendar (Rendtel, 2021). The (predicted) times are:
May 31, 04:55 UT ($\lambda_\odot = 69\overset{\circ}{.}44$; min. dist. +0.0004 au; Jenniskens 2006, quoting Lüthen et al. 2001),
May 31, 05:17 UT ($\lambda_\odot = 69\overset{\circ}{.}459$; −0.00214 au; Jenniskens 2006),
May 31, 05:04 UT ($\lambda_\odot = 69\overset{\circ}{.}451$; −0.00041 au; Sato 2021).
Sato commented "the density of the trail is estimated to be low because of the large ejection velocity. However, we may be able to see a meteor storm [...] because a lot of dust is expected due to the breakup". Another very late calculation by Vaubaillon[a] yielded a peak centered at 05^h01^m UT. Additionally, the Earth was expected to encounter SW3-dust mainly ejected in 1892 and 1897 (Wiegert et al., 2005). The diagram shown in this paper indicates an encounter of the 1897 meteoroids near 16^h UT and of the more widely scattered 1892 meteoroids close to 02^h UT.

Therefore all observations between May 30, about 16^h UT and May 31, about 07^h UT were of essential interest. Some of the questions which possibly can be answered from analyses of visual data are:

- times of ZHR maxima, especially the main peak,
- strength of the ZHR maxima,
- difference in the magnitude distributions (population index r),
- correlation between ZHR and r,
- number density in the different regions of the stream.

It is not possible to observe the entire period of interest from one location on Earth. At the end of May, the number of dark hours in the northern hemisphere is rather short and observers north of about 55° N cannot observe at all. Locations in wide parts of North America were favourable to observe the main peak. European locations allowed to follow part of the early activity. Depending on the latitude, the dark window was quite short. From the Canary Islands it was possible to observe for 8 hours and thus to see a part of the early activity as well as the time until the main peak. We found that 05:10 UT is the latest moment for useful data when the western sky is still reasonably dark while the the eastern sky has already bright twilight. Additionally, the radiant elevation decreases a lot towards the morning. Hence all effects around the zenith attraction za (see Koschack et al., 2022) and zenith coefficient γ (see Bellot Rubio, 1995) are of great importance. Our own short campaign on Tenerife from May 28 to June 1 with four clear nights in a row was successful and contributed data for the maximum night as well as from the neighbouring nights for calibration purposes. This allows us to have a closer look at the radiant change due to gravitation effects but not on the zenith coefficient question.

2 Visual observations worldwide

The IMO's VMDB received reports from 45 visual observers covering the period from May 25 to June 3 (with the vast majority of reports from the maximum

[1]Leibniz-Institut f. Astrophysik Potsdam, An der Sternwarte 16, 14482 Potsdam, Germany. Email: jrendtel@web.de
[2]International Meteor Organization, Eschenweg 16, 14476 Potsdam, Germany.

IMO bibcode WGN-503–4-rendtel-tah
NASA-ADS bibcode 2022JIMO...50...92R

[a]https://www.imcce.fr/recherche/campagnes-observations/meteors/2022the, (accessed 2022 July 11)

night May 30/31), including data of 1661 shower meteors. Here we list the observers and their observing region as well as the number of session reports submitted:

Mark Adams (USA, 3 sessions); Daniel Alcázar (Spain, 1); Rainer Arlt (Spain, 4); Orlando Benítez Sánchez (Spain, 1); Tim Cooper (South Africa, 1); Howard Edin (USA, 1); Christoph Gerber (Germany, 1); Robert Harris (USA,1); Jan Hattenbach (Spain, 1); Carl Hergenrother (USA, 1); Glenn Hughes (Australia, 9); Javor Kac (USA, 2); André Knöfel (Germany, 1); Pete Kozich (USA, 1); Jens Lacorne (France, 1); Anna Levin (Israel, 1); Michael Linnolt (USA, 1); Robert Lunsford (USA, 3); Oleksandr Maidyk (Ukraine, 1); Oscar Martin Mesonero (Spain, 1); Pierre Martin (Canada, 2); Marco Micheli (Italy, 1); Russell Milton (USA, 2); Koen Miskotte (France, 6); Sirko Molau (USA, 1); Edward Murphy (USA, 1); Basil Nikolau (USA, 1); Artyom Novichonok (Russia, 3); Francisco Ocaña González (USA, 2); Sasha Prokofyev (Cyprus, 4); Ina Rendtel (Germany, 3); Jürgen Rendtel (Germany, Spain, 6); Terrence Ross (USA, 3); Ivan Sergey (Belarus, 4); Wesley Stone (USA, 1); Fengwu Sun (USA, 1); Hanjie Tan (Czech Republic, 1); Austin Uhler (USA, 1); Michel Vandeputte (Belgium, 1); Alan Webb (USA, 2); Thomas Weiland (USA, 1); Frank Wächter (Germany, 1); Sabine Wächter (Germany, 2); Quanzhi Ye (USA, 1)

The nights May 28/29 to May 31/June 1 are well covered, and we have a continuous data series from May 30, $21^{\rm h}$ UT, to May 31, close to $12^{\rm h}$ UT. This allows us to analyse the points raised in the Introduction. A first look into the data, e.g. as provided by the IMO live graph, shows a ZHR profile with a main peak near $05^{\rm h}15^{\rm m}$ UT. Additionally, we find an earlier and much weaker maximum close to May 30, $23^{\rm h}$ UT. It may be tentatively associated with the meteoroids released from the comet around the perihelia in 1892 and 1897.

In order to obtain complete information, we first analyse the magnitude data before dealing with the ZHR and spatial number density. Due to the very low entry velocity, the visual meteors represent a mass range which considerably differs from (most of) the known meteor showers. The consequences are described below.

3 Population index r

The ZHR calculation requires the knowledge of the population index r to correct for the standard conditions (see, in detail, Koschack et al., 2022). The available observing reports cover the period between May 30, $21^{\rm h}$ UT, and May 31, $12^{\rm h}$ UT quite well. The geographical distribution of the observers between Eastern Europe and Western North America as listed above ensures that we have magnitude (and rate) data with high radiant position available for the entire period.

First, we calculated a general value of the population index for the shower including both the main peak of fresh meteoroids and the early activity period caused by meteoroids released about a hundred years earlier. The general average is $r = 2.40 \pm 0.06$ centred at $\lambda_\odot = 69\,^\circ\!.407$ and is based on magnitude data of 1521 TAH meteors (245 intervals with magnitude distributions).

Next, we checked whether there is a difference between the main activity period and the period before. The respective values are: old meteoroids $r = 2.57 \pm 0.23$ centred at $\lambda_\odot = 69\,^\circ\!.198$ and fresh meteoroids $r = 2.38 \pm 0.06$ centred at $\lambda_\odot = 69\,^\circ\!.455$.

It seems the values further to the edges are slightly higher. We find $r = 2.81 \pm 0.67$ at $\lambda_\odot = 68\,^\circ\!.36$ (only based on magnitude data of 35 TAH), and $r = 2.44 \pm 0.92$ at $\lambda_\odot = 70\,^\circ\!.15$ (17 shower meteors).

The two values for old and fresh indicate that there is a small difference in the meteoroid size distribution between the fresh material and the meteoroids ejected earlier. However, the difference is not remarkably large.

One of the main questions for the 2022 activity was, whether meteoroids were able to reach the Earth because the "standard ejection conditions" would have hardly brought meteoroids released as a consequence of the 1995 comet breakup to Earth encounters (see the remarks in the Introduction and at the IMCCE website quoted above). A higher ejection speed was required, but it seemed open what size the encountering meteoroids would have. A question, which was of great importance because of the low velocity of the TAH meteors.

The observed meteor magnitude range (Table 1) between −3 and +5 mag translates into a mass range between 170 g (!) and 0.06 g. Meteoroids of the same mass range would appear as meteors of −6.1 and +1.6 mag, respectively, when entering the atmosphere at 35 km/s (Geminids), and much brighter if apearing as Perseids. This means, that the bright Tau Herculids (of −2 or −3 mag) which we saw particularly around the peak (Table 2) were quite large meteoroids which are not frequent in other showers. The reported magnitude distributions include rather few +6 magnitude TAH meteors in the magnitude data. This is a bit surprising because the original expectation was that we may see a

Table 1 – Magnitudes of the observed Tau Herculid meteors in different periods. The first line gives the total of all TAH meteors from reported between May 24 to June 4; the subsequent lines (labelled 'Max.') give details for periods of the maximum night May 30/31. There is one −6 TAH meteor which was seen by two observers at the same site. Two session reports summarised the magnitude data over 2.5 and 3.0 hours, respectively, and are not considered in the separate pre- / post-peak distributions.

Sample	−6	−5	−4	−3	−2	−1	0	+1	+2	+3	+4	+5	+6
All TAH meteors	2	0	2	8	12.5	33	84	204	277.5	412.5	448	298.5	30
Max. $19^{\rm h}$–$02^{\rm h}$UT	0	0	0	0	1.5	2.5	8.5	24.5	26.5	41	74.5	38.5	10.5
Max. $02^{\rm h}$–$05^{\rm h}$UT	0	0	1	5	2	16.5	34	73.5	115.5	195	184	131	9.5
Max. $05^{\rm h}$–$11^{\rm h}$UT	2	0	1	3	7	11	37.5	92	115.5	158	156	110	8

Table 2 – Appearance of bright Tau Herculids TAH_B (here: −2 mag and brighter) in different sections of the activity profile close to the maximum on 2022 May 30/31. The time given here is the total effective observing time of all observers contributing to the sample. The −6 mag TAH meteor observed near 06^h30^m UT is one of the "4" in the line 0600–0700 UT although referring to one single fireball (reducing the TAH_B to 0.30 if counted as just one bright TAH).

Period (UT)	#TAH_B	Eff. obs. time (total, hrs)	TAH_B/hr
< 11	0		0
1940–0200	1.5	27.2	0.055
0200–0300	0	2.5	0
0300–0400	3	12.0	0.25
0400–0500	4	15.1	0.27
0500–0520	5	4.9	1.02
0520–0600	0	10.7	0
0600–0700	4	10.1	0.40
0700–0800	1	4.7	0.22
> 08	0	7.8	0

shower rich in faint meteors due to the low velocity. So the visual data raise the opposite question, whether the comet mainly released larger meteoroids (in the recent breakup ejection as well as in the older material) – or whether this is an observers' bias. The latter seems unlikely, as the apparent lack of +6 TAH meteors is found throughout the entire activity period.

The amount of magnitude data allows us to try looking for details within the two "activity periods", i.e. for structures in the stream. We adjusted the binning lengths for the *r*-calculation throughout the entire period. For the interval 69.°13 to 69.°35 (about 21^h UT to 02^h30^m UT) we used bins of 0.°08 shifted by 0.°04 (giving a temporal resolution of 1 hour). The large number of data around the main peak allowed us to set the bin length 0.°04 shifted by 0.°02 (30 minute resolution). The result is shown in Figure 1.

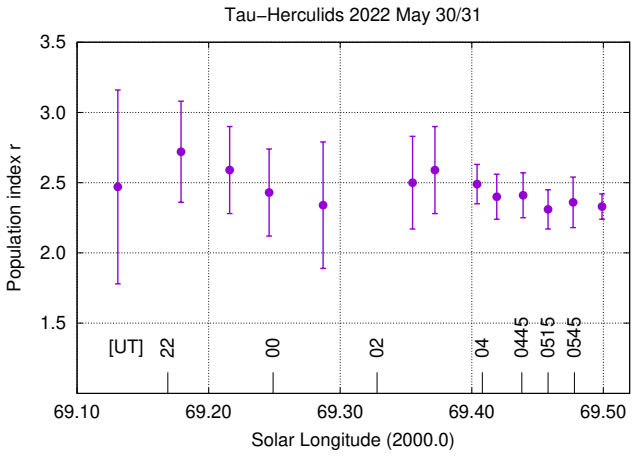

Figure 1 – Population index *r* of the Tau Herculids during the night 2022 May 30-31 with 1-hour resolution before 02^h UT and 30-minute resolution around the peak (see the bin lengths given in the text). The much larger error margins before 02^h UT are caused by the smaller sample available for this period of lower activity.

Encouraged by this surprisingly smooth profile, we tried even shorter bins, being aware that the error margins and uncertainties become much larger. Nevertheless we think that the profile with 10 minute bins (0.°007) has some information. An inspection of the magnitudes of bright shower meteors revealed that there was a kind of stop at 05^h15^m UT or immediately after that. Before this, a significant number of −2 to −3 mag meteors was reported, but almost none in the period after that. However, a change of the population index from 2.26 to 2.50 from one 10-minute interval to the next occurs only after 05^h30^m UT. Like all the variations we see in the profile shown in Figure 2, the error margins indicate that cannot draw conclusions from any feature – even if we find confirmation by other data series.

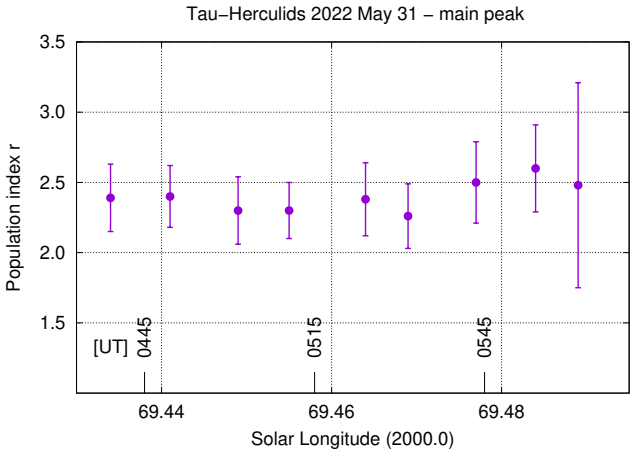

Figure 2 – Attempt to derive a population index *r* profile of the Tau Herculids with higher temporal resolution (10 minutes) during the main peak period. Details are given in the text. The variations are rather small and we cannot find features in the profile.

4 ZHR profile

For the calculation of the ZHR values we applied the *r*-profile shown in Figure 1. A large fraction of the observers had good observing conditions (limiting magnitude +6 or better) so that a difference of say 0.1 of the population index does not affect the resulting ZHRs too much. The result of the ZHR calculation is shown in Figure 3. Like in the case of the population index, the smaller sample for intervals when the old TAH meteoroids occurred, we also used longer bins for the ZHR calculation.

There are two obvious features in the ZHR profile: a sharp and pronounced peak with a ZHR = 55 ± 7 at 05^h05^m UT (±5 min) and a rather broad maximum with a ZHR = 18±3 centred at 23^h UT. The main peak has a skew shape. The ZHR reaches half the peak value (25) near 02^h40^m UT (duration 2.5 hours) and the descend to the same ZHR happens close to 06^h30^m UT (duration 1.3 hours). From our data we cannot see whether the longer ascend is a characteristic of the distribution of the fresh meteoroids or a superposition with probable older material. This may perhaps be distinguished from orbital data.

The early maximum with a ZHR just below 20 most

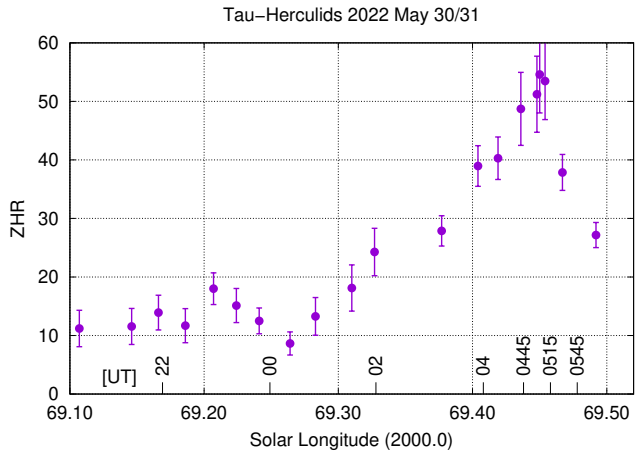

Figure 3 – ZHR-profile of the Tau Herculids during the night 2022 May 30-31, using the population index profile shown in Figure 1. The peak occurred at $\lambda_\odot = 69\overset{\circ}{.}450$, on May 31, 05^h05^m UT. An earlier maximum is found at $\lambda_\odot = 69\overset{\circ}{.}207$, on May 30, 23^h UT.

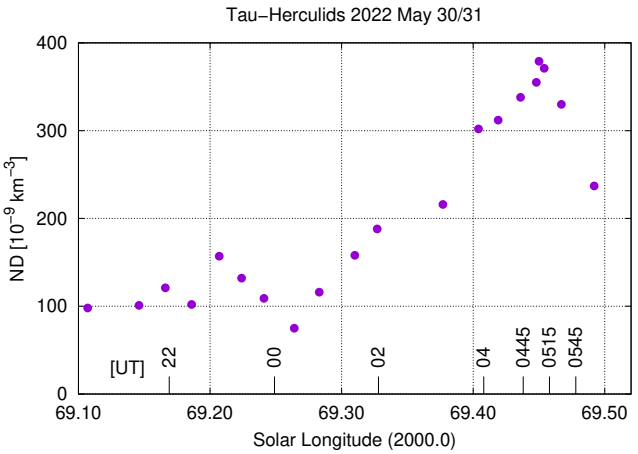

Figure 4 – Profile of the spatial number density of the Tau Herculids during the night 2022 May 30-31, based on the ZHR profile shown above and the population index as shown in Figure 1.

likely is caused by meteoroids from the old particle releases. Considering the diagram shown in Wiegert et al. (2005), the broader scattered 1892 meteoroids are more likely the cause for the maximum we find around 23^h UT. We may estimate a width of this maximum of about 3 hours, but as the end seems to overlap with the starting ascend to the main peak, this is somewhat uncertain.

5 Number density

As pointed out above, the TAH meteor brighnesses up to −2 to −3 magnitude (very few meteors even brighter than that!) and the low atmospheric entry velocity are equivalent to rather large meteoroid masses. The number density, which is the better suited quantity to compare meteoroid streams than the ZHR (which describes the appearance of the shower in the observer's sky), is remarkably high (Figure 4).

The Geminids with a ZHR of about 150 are caused by a meteoroid stream with a spatial number density ND $\approx 200 \times 10^{-9}\mathrm{km}^{-3}$ for meteoroids larger than 1 mg; the corresponding value for the Tau Herculid peak is about $380 \times 10^{-9}\mathrm{km}^{-3}$ – for meteoroids larger than 10 mg (we do not have fainter meteors / smaller meteoroids in our sample). So the TAH shower is about twice as dense as the Geminids. Not to imagine the impression if the Earth would enter such a stream at Perseid speed.

6 Some thoughts on the zenith correction

The correction of observed meteor rates to a situation in which the shower radiant is in the zenith has been a long-standing issue. For meteoroids on parallel trajectories hitting a plane "detector", it is $\sin^{-1} h_\mathrm{R}$, where h_R is the elevation of the radiant above that plane. Various attempts have included the curvature of the Earth's surface, which in principle allows for meteors becoming visible if the radiant is slightly below the horizon. The issue was treated by, e.g., Kresák (1954) and Richardson (1999). Both authors appear to take the apparent radiant elevation as the relevant quantity to compute the zenith correction factor.

The apparent radiant is the one resulting from the vector addition of the orbital motions of the stream particles and the Earth, plus the shift of the radiant towards the zenith due to the gravitational attraction of the particles by the Earth, before they light up as meteors in the atmosphere. This shift is individual to each observer location and time and needs to be computed for each observing period. (There is also another velocity vector of the observer which needs to be added to the radiant direction. It results from the rotation of the Earth and is called diurnal aberration, but has very small effects on the corrections of visual observations.)

Whether the zenith corrections needs to be based on the apparent radiant is not entirely obvious. The question comes down to asking: does a detector on Earth record the same number of particles from a shower with apparent radiant elevation h_A, i.e. *after* gravitational attraction, as a detector in space without gravity and therefore entirely geometrical radiant angle h_R which is equal to h_A? In other words, does the zenith attraction simply change the direction of the particle flux vector without affecting the absolute flux?

As demonstrated by Gural (2001), the radiant of particles ideally moving in parallel at infinity (radiant an ideal point without gravitational attraction) becomes an area of 4–5 degrees at geocentric velocities like the ones of the tau Herculids. The zenith-attracted radiant locations depend on the locations of particles in three-dimensional space and it may well be that their flux is lower than that of a hypothetical shower unaffected by gravity whose radiant location is equal to the mean zenith-attracted radiant of the real shower. The meteor simulation code by Gural (2002) – employed to e.g. the Leonid shower by Molau et al. (2002) – would be the ideal tool for exploring this question.

To evaluate the effect, we compared a few individual interval data of the present Tau Herculid data of May 31. The zenith distance of the observed radiant

Table 3 – Effect of the zenith correction on the ZHR on 2022 May 31, between 04^h and 05^h05^m UT. We averaged the individual ZHR values for observers on locations on the Canary Islands (CI) and on various locations in North America (NA). h_R is the geometric radiant elevation; h_A the apparent elevation due to the Earth's gravitiation.

Period (UT)	Intervals (CI)	Radiant h_R	ZHR (avg.)	Radiant h_A	ZHR(CI) (avg.)	ZHR(NA) (avg.)
0407–0425	3	12°–17°	64	26°–28°	38	41
0437–0505	6	5°–12°	76	17°–23°	37	52

z_O affected by the zenith attraction is calculated by $z_O = \frac{z_t}{2} + \arcsin\left(\frac{v_g}{v_\infty}\sin\frac{z_t}{2}\right)$ where z_t is the (geometrical, undisturbed) zenith distance of the radiant, v_g and v_∞ are the velocities before and after the Earth gravitation (for the full details of radiant corrections see Gural, 2001). In the present case $v_g = 12.36$ km/s and $v_\infty = 16.61$ km/s.

For this purpose we find the data recorded from the Canary Islands (CI) and from locations in North America (NA) very useful. They overlap during the period between 04^h UT and 05^h15^m UT, when the radiant was low in the western sky as seen from the CI (see Figure 5) and near zenith in NA much further west. So the NA data provide the undisturbed ZHR values, and we compare them with the strongly corrected ones (Table 3). The values may suggest that applying the shifted radiant position is too strong. But this is just for a handful numbers and the scatter is enormous. It just demonstrates that the effect is present and the correction acts in the right direction and reliable order of magnitude.

At this point, we emphasize that the quantitative assessment of the zenith correction at very low geocentric meteoroid velocities and very low radiant positions goes beyond the scope of the present paper.

7 Discussion

The visual Tau Herculid observations in 2022 allowed us to document the activity of the encounter in great detail. We find two obvious activity maxima. An early maximum (ZHR = 18 ± 3 centred at May 30, 23^h UT) is probably caused by meteoroids released from SW3 in 1892. The observed maximum is roughly 3 hours before the position which is indicated by the modelling (Wiegert et al., 2005). But the meteoroids of this ejection period seem be be scattered over a large range as compared to the main peak.

Unfortunately, we do not have visual data covering the period around 16^h UT on May 30, when the Earth may have encountered the 1897 SW3-ejecta (again, as modelled).

The main peak occurred at $\lambda_\odot = 69\,^\circ\!.450$ corresponding to 05^h05^m UT (±5 minutes) with a ZHR = 55 ± 7. Its shape is skew with a longer ascend than the subsequent descend. From our data we cannot decide at which moment the fresh particle population dominates the observed sample. This may be distinguishable from orbital data. The population index r is slightly higher before or outside the fresh meteoroid range. The difference in r is not really large: 2.57 vs. 2.38. The population index, however, is in the range of other meteor showers. This was not to be expected because a similar particle size distribution to other showers should have resulted in a shower with mainly faint meteors. A large portion of faint TAH meteors was to some extent anticipated but did not happen. Just the opposite: the fresh ejecta from SW3 seem to be larger than average. Perhaps the short duration from the ejection to the observed encounter kept the large meteoroids which may disintegrate with time. If the original size distribution was similar during the 1892/1897 ejections, the difference in r may give a hint at the disintegration process. Perhaps the 1995 SW3 disintegration was unique as it caused large areas of fresh exposed comet surface and releasing an untypical meteoroid sample.

8 Conclusions

8.1 Observational data

The encounter with the fresh meteoroids was highly anticipated and gained huge attention. Since it was not clear in advance, what level of activity would occur, observers took a lot of effort to collect data applying all techniques.

8.2 Observed ZHR

We find two maxima: a pronounced peak ZHR = 55 ± 7 05^h05^m UT ($\lambda_\odot = 69\,^\circ\!.450$) lasting 3.8 hours (2.5 hours ascend, 1.3 hours descend). It is caused by the 1995 ejecta from SW3 and occurred closest to Sato's and Vaubaillon's most recent prediction (see Introduction). A broad maximum with a ZHR = 18 ± 3 occurred at 23^h UT ($\lambda_\odot = 69\,^\circ\!.207$); this maximum is about 3 hours wide. It may be associated with dust ejected at the end of the 19th century, but seems to deviate from the modelled distribution as shown in Wiegert et al. (2005) – it is earlier than the probably centre of the 1892 dust.

8.3 Population index and meteoroid masses

The population index r is in the same range as for other meteor showers and therefore much lower than expected in advance. We do not see any peculiar change in r around the main peak of fresh meteoroids, but an indication of more bright (of at least −2 mag) shower meteors in the immediate vicinity of the peak. The size distribution of the fresh ejecta as well as those released in 1892/97 are not much differing. However, the sizes of the TAH-meteoroids differ considerably from average size distributions found in annual meteor showers.

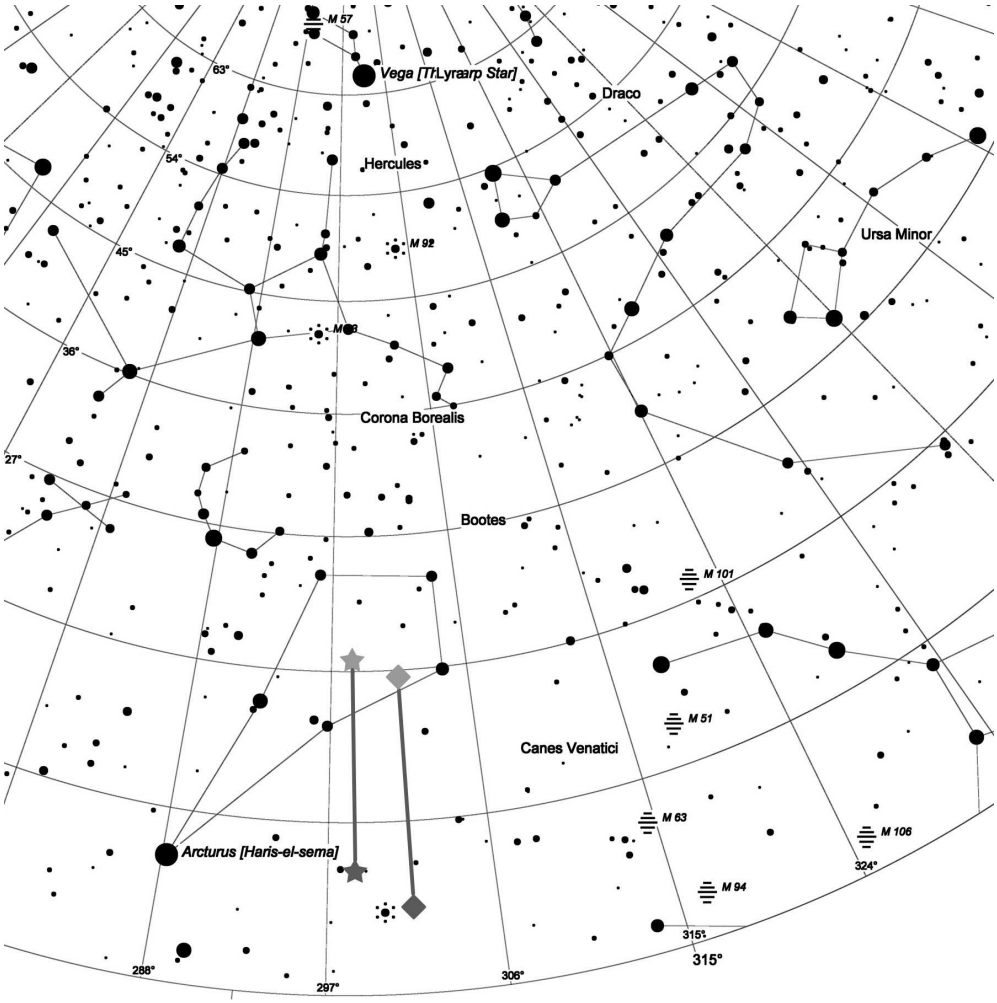

Figure 5 – Shift of the shower radiant due to the zenith attraction. The setting shown here is for Izaña, Tenerife, on 2022 May 31, 05^{h} UT. The velocities used are $v_g = 12.36$ km/s (Jenniskens, 2006), $v_{\mathrm{inf}} = 16.61$ km/s (as converted with the Gural (2001) correction). The radiant shift shown as stars refer to the data provided for the 2022 Shower Calendar (Rendtel, 2021) by Sato (personal communication) and Vaubaillon (repeated shortly before the event at `https://www.imcce.fr/recherche/campagnes-observations/meteors/2022the`), while the the diamonds show the radiant from Lüthen et al. (2001).

8.4 Number density

A ZHR of the order of 50 usually does not indicate that the Earth passes a dense stream. Together with the low velocity and the average r, we indeed find a dense stream (ND $\approx 380 \times 10^{-9}\mathrm{km}^{-3}$) for particles of at least 10 mg which has about twice the spatial number density of the Geminid peak (ND $\approx 200 \times 10^{-9}\mathrm{km}^{-3}$; m ≥ 1 mg).

8.5 Zenith attraction effects

We briefly discuss in which way the meteoroid trajectories modified by the Earth's gravitation further affect the determination of the ZHR and flux density. A few data obtained under different geometrical conditions indicate that the corrected radiant position needs to be applied for the ZHR (and subsequent flux density) calculation, although we cannot conclusively answer this question in this paper.

9 Acknowledgements

We thank all visual observers for submitting their data to the IMO's VMDB. This data flow happened very fast so that we were able to adjust the parameters continuously through the activity period. Therefore, the live graph indeed was a good display of the TAH activity.

References

Bellot Rubio L. R. (1995). "Effects of a dependence of meteor brightness on the entry angle". *Astronomy & Astrophysics*, **301**, 602.

Gural P. S. (2001). "Fully Correcting for the Spread in Meteor Radiant Positions Due to Gravitational Attraction". *WGN, Journal of the International Meteor Organization*, **29:4**, 134–138.

Gural P. S. (2002). "Meteor Observation Simulation Tool". In Triglav M., Knöfel A., and Trayner C., editors, *Proceedings of the International Meteor Con-*

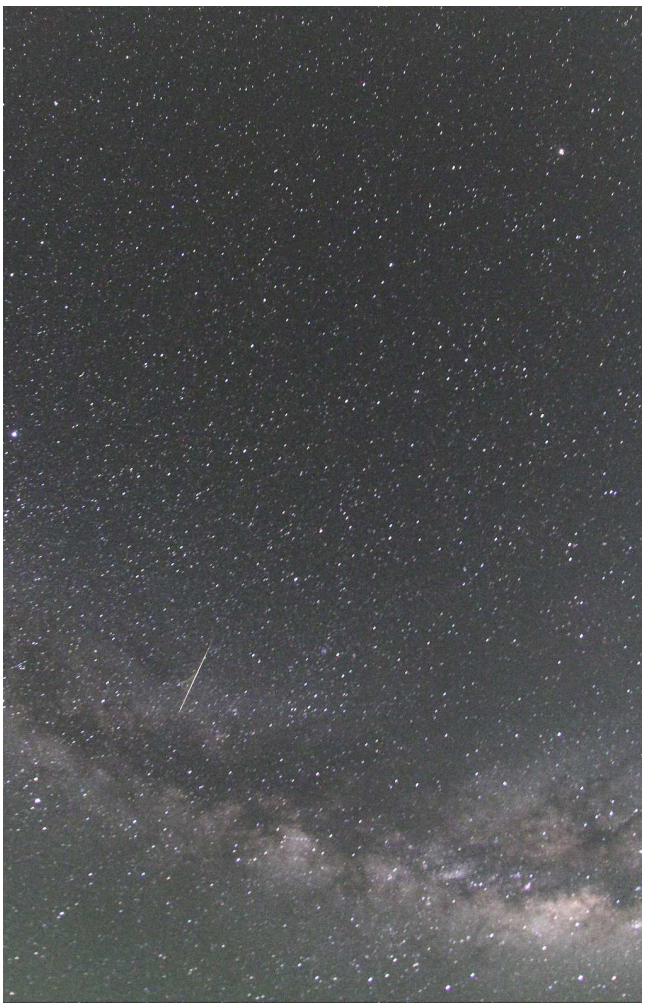

Figure 6 – Photo of a Tau Herculid meteor taken from Tenerife on 2022 May 31, $01^{h}11^{m}$ UT. The backward prolongation of this −2 mag meteor already points to a position north of the undisturbed radiant although it appeared about 4 hours before the setting shown in Figure 5. The image was taken with a fish eye lens, $f = 8$ mm, $f/d = 4$, exposed 59 seconds; Canon EOS60Da.

ference, 20th IMC, Cerkno, Slovenia, 2001. pages 29–35.

Jenniskens P. (2014). "Camelopardalids (IAU#451) from comet 209P/LINEAR". *WGN, Journal of the International Meteor Organization*, **42:3**, 98–105.

Koschack R., Rendtel J., and Richter J. (2022). "Analyses and calculations". In Rendtel J., editor, *Handbook for meteor observers*, page 180.

Kresák L. (1954). "On a Criterion Concerning the Perturbing Action of the Earth on Meteor Streams". *Bulletin of the Astronomical Institutes of Czechoslovakia*, **5**, 45.

Lüthen H., Arlt R., and Jäger M. (2001). "The Disintegrating Comet 73P/Schwassmann-Wachmann 3 and Its Meteors". *WGN, Journal of the International Meteor Organization*, **29**, 15–28.

Molau S., Gural P. S., and Okamura O. (2002). "Comparison of the "American" and the "Asian" 2001 Leonid Meteor Storm". *WGN, Journal of the International Meteor Organization*, **30**, 3–21.

Rao J. (2021). "Will Comet 73P/Schwassman-Wachmann 3 produce a meteor outburst in 2022?". *WGN, Journal of the International Meteor Organization*, **49:1**, 3–14.

Rendtel J., editor (2021). *2022 Meteor Shower Calendar*. International Meteor Organization. IMO_INFO 2-21.

Richardson J. (1999). "A Detailed Analysis of the Geometric Shower Radiant Altitude Correction Factor". *WGN, Journal of the International Meteor Organization*, **27:6**, 308–317.

Wiegert P. A., Brown P. G., Vaubaillon J., and Schijns H. (2005). "The τ Herculid meteor shower and Comet 73P/Schwassmann-Wachmann 3". *MNRAS*, **361:2**, 638–644.

Handling Editor: Javor Kac
This paper has been typeset from a LaTeX file prepared by the authors.

27 Tau Herculids in 2:18 hours from a subclass observation site

Peter C. Slansky[1]

A short report about observation with a camera and an attempt of visual observation from Munich, Germany, is presented.

Received 2022 July 2

The announcement of extraordinary Tau Herculids' activity in 2022 induced little hope to me because University duties tied me to Munich on the time around 31st of May. All I could do was to set up a camera on my roof top terrace in the Munich city centre and try to see some meteors in parallel – and get some sleep before my lectures next morning. My camera was a Sony Alpha 7S with a Sony 1.4/24 mm lens on a tripod connected to a UHD video recorder Atomos Ninja V. "UHD" means a resolution of 3840 × 2160 pixels. The a7S can give out this resolution via its HDMI 1.4 output at 25 fps. Record button was pushed at $23^{h}49^{m}$ CEST ($21^{h}49^{m}$ UT). In parallel I observed visually, looking to the zenith. Due to the Munich city centre sky illumination the visual stellar limiting magnitude was quite poor. The camera/lens had to be set to ISO 51 000 at $^{1}/_{25}$ s exposure time and $F = 2.0$. During one hour of observing time, from midnight to $01^{h}00^{m}$ CEST, my visual meteor recovery was exactly ZERO. With little hope I started video inspection on a 52" OLED UHD flat screen in a complete dark room at my university.

But to my surprise the limiting magnitude in my video was about +7 mag, and I found 44 meteors in $2^{h}18^{m}$ video recording, 27 of them Tau Herculids. The brighter meteors came after the end of my visual observation but I was still astonished to find 16 meteors in the video that had been exactly inside my visual field of view. It reveals the superiority of meteor video observation over visual observation, even (or especially?) under poor sky quality.

From this video I created a composite image in Photoshop with 22 Tau Herculids. 5 TAHs had to be left out because they were outside the field of view of the sky background which was generated in the middle of the observing time. Again, UHD resolution pays off: the meteor streaks are much more filigree than with Full HD resolution. Even the double radiant that was reported by an observer from Texas is visible. So, I do not envy the observers who saw the maxima in the US or elsewhere (well, only a little bit. . .).

[1]Email: slansky@mnet-online.de

Handling Editor: Javor Kac

IMO bibcode WGN-503–4-slansky-tah
NASA-ADS bibcode 2022JIMO...50...99S

Figure 1 – Inverted composite image of 22 Tau Herculids observed from from Munich city centre on 2022 May 31 between $22^{h}01^{m}$ and $00^{h}01^{m}$ UT. Camera: Sony a7S at ISO 51 000 and 25 fps with Sony GM 1.4/24mm lens at $F = 2.0$ and external UHD recorder Atomos Ninja V. North is left. Please find the original, non-inverted version of the image here: https://www.imo.net/members/imo_photo/view?photo_id=2407.

Analysis of Video Observations from the Tau Herculids on May 30, 2022

Mario K. [1]

The 2022 Tau Herculids were observed from Germany with two video cameras. Analysis of the data is presented.

Received 2022 July 17

1 "Short" Preface

Last fall I realized, that the two cameras Nikon Z50 (APS-C format) and Nikon Z6II (full-frame) allow to record meteors in 4k format (3840×2160) with 25 fps (as mp4 and in b/w). However, the detection and analysis of meteors in the video footage is quite time-consuming:

1. After 8 hours of office work I am typically too tired to search patiently for meteors (I still have unprocessed video recordings from two December nights).
2. The monitor requires different settings depending on the camera, video type, time, and distance to monitor. The noise is particularly disturbing for the Z50 camera with strong contrast.
3. The same holds to the VLC media player that I use for playback. You can jump forward frame-by-frame, but only in steps of 1 s backward.
4. Trajectory determination is done with Stellarium (`https://stellarium.org/`) in such a way, that one monitor shows the video, and another monitor a star map in gnomonic projection. I determine the path of meteors with a ruler using fainter stars for orientation. That is quite time-consuming. After a short time I gave up to measure the coordinates of the begin and end points, even though the accuracy was better than 0.1° for the full-frame camera according to the astronomy program.
5. The brightness estimation is tedious as well. Due to scintillation of stars, they have a different brightness in different frames. Also, the color of stars has a negative effect, as well as vignetting of the lens.

Last not least, 4K videos are getting quite large: 26 GB for 30 minutes. You cannot even store five films on a 128 GB memory card. And the videos have to be transferred to the computer – during the observation with two rotating memory cards.

Since my observations are neither suitable as visual, nor as database-ready video observation, I did not further record meteor shows – with the exception of the Quadrantids.

However, for the tau Herculids I have resumed my activities. Nights are short in Berlin at the end of May, which limits the recording time. TAH meteors are slow, which could make the analysis easier, and higher replay rates reduce the noise.

[1]Berlin, AKM e.V.

IMO bibcode WGN-503–4-mariok-tah
NASA-ADS bibcode 2022JIMO...50..100M

2 Observation on May 30, 2022

According to the weather forecast, there should have been an interval with clear skies after lower clouds have dissipated and higher clouds would arrive. During the observation, some lower clouds arrived from the western direction, but they dissipated partly at the western city boundary and partly in the field of view.

The Z6II camera started recording at $20^{h}54^{m}$, the Z50 camera at $21^{h}03^{m}$ (all times UT). Between $22^{h}05^{m}$ and $22^{h}29^{m}$, some lower clouds drifted through the field of view, and observation was terminated by another patch of low clouds before the Cirrus arrived. In total the cameras recorded for $1^{h}50^{m}$, but only 1 hour was free of clouds.

3 Camera setup

I mounted both cameras at a balcony, which is meanwhile not possible anymore because of flowers. So I photographed the setup later in a room (Figure 1).

The camera mount was a bit adventurous. In particular shaky was the combination of different components with different age for the Z50 camera. While fixing the screws, the field of view got somewhat misaligned with respect to the horizon.

Figure 1 – Camera setup (here for illustration in a room): left the Z50 camera with 1.8/20 mm lens, right the Z6II camera with 1.8/50 mm lens.

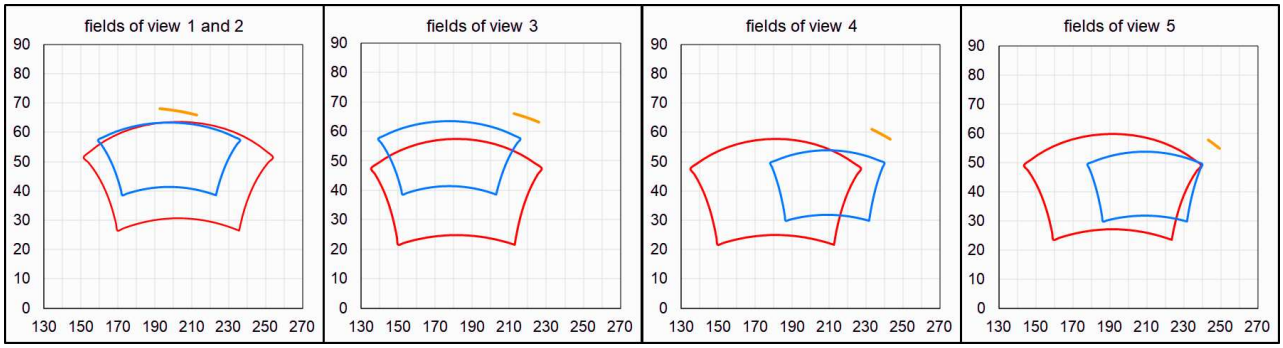

Figure 2 – Fields of view (azimuth and altitude) of the two cameras and the motion of the TAH radiant during the observation (orange line).

I selected the balcony facing south/south-west, since the northern skies was too bright at the begin of observation, and the predicted faint TAH meteors with short trails should be easier visible there.

For the five time intervals with suitable recordings, you see in Figure 2 the fields of view of the two cameras (blue = Z6II with 1.8/50 mm lens; red = Z50 with 1.8/20 mm lens) and the position of the TAH radiant (orange line) corrected for zenith attraction in azimuth and altitude.

The fully open 1.8/50 mm full-frame lens has a vignetting of 0.9 f-stops at the edges of a full-frame sensor, in smaller videos formats a little less.

The fully open 1.8/20 mm full-frame lens shows the same effect in the APS-C format, but by a smaller amount. The strongly distorted edges, which are clearly visible in the full-frame camera, are outside the fov of the APS-C sensor.

It is obvious, that the fields of view overlap and have different sizes (Z50: $58.2° \times 32.8°$; Z6II: $39.1° \times 22.0°$). I wanted to let the Z50 camera fully cover the field of the Z6II camera, but that was not possible due to clouds and my plan to keep the Z6II field near the radiant.

In the observing intervals 1, 2 and 5, the FOV of the Z50 camera covers most of the Z6II camera FOV. In the other two intervals, it covers about 2/3 of it.

4 Meteor Detection at the Monitor

I adjusted the monitor and VLC player settings to maximize the contrast, but leave the noise at an acceptable level.

The determination of the limiting magnitude is nearly impossible, because it depends from:

- my mental fitness (I am not a computer program),
- the monitor settings and distance,
- the replay speed,
- strewn light from the upcoming clouds,
- cloud that are dissipating inside the field of view.

For the Z50 camera I estimated LM from 5.5 mag at the beginning and in times with cloud interference to 6.0 mag. For the Z6II camera the LM ranged from 7.0 to 8.0 mag. When watching the video in double-speed to determine the coordinates of the center of FOV, the limiting magnitude improved by 2 mag.

For the estimation of the meteor brightness, I expect errors of the order of 1 mag.

The evening twilight at the begin of night (solar altitude $-9.8°$) was less disturbing than the many satellites. Up to ten of them were visible in parallel when watching the video in double speed. I was also distracted by bats and moths, and by cosmics in case of the Z50 camera.

For the first inspection of videos, I replayed at double-speed, which reduced the noise significantly. However, this way I was also missing particularly weak and short meteors.

By watching the video multiple times – also at normal speed – I could find more meteors. Since I detected the faintest ones only by directly looking at them, I will still have missed a few of them. In fact, while preparing this paper, I found still a few more meteors.

5 Analysis of Observation

In total, I could record 56 meteors with the Z50 camera, 48 of them being TAH. With the Z6II camera I recorded 54 meteors, 41 TAH among them.

Ignoring double recordings (Z50 and Z6II) I counted 69 TAH, 2 ANT and 16 SPO. Figure 3 shows the temporal distribution and the brightness of these meteors. Figure 4 depicts separated for both cameras the temporal distribution and the brightness of TAH meteors. Double detections are now visible.

In addition, some of the meteors came in short succession showing about the same magnitude.

For the following analyses (separated for both cameras) I omitted ANT and SPO. Data from the Z50 camera are shown in red, for the Z6II camera in blue.

5.1 Brightness Distribution

Even though it would have been possible to determine the brightness with 0.5 mag resolution, I rounded to full mags because of the uncertainties in the estimation described earlier. Figure 5 shows the brightness distribution of meteors for both cameras separately.

The distribution of the Z50 camera shows a peak at 4 mag, the Z6II camera at 5 and 6 mag. That is not surprising because the limiting magnitude was reduced at the begin of observation and temporarily when lower clouds passed the field of view.

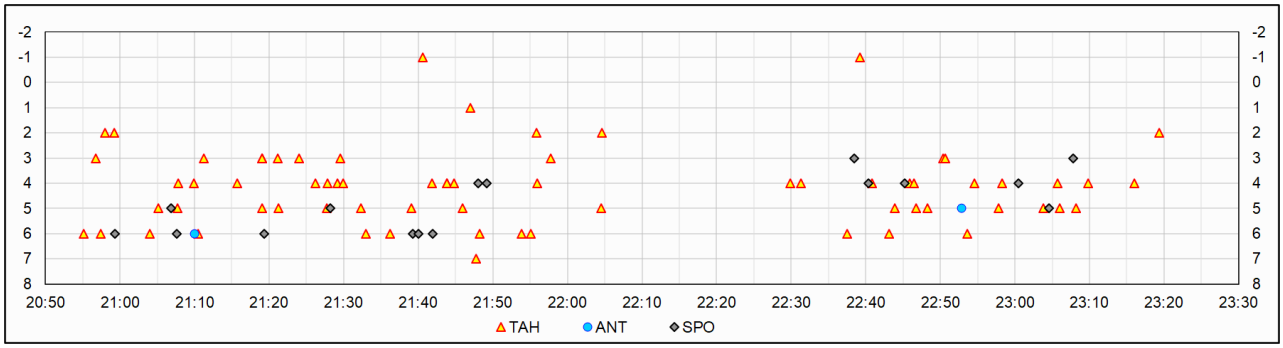

Figure 3 – Temporal distribution of all meteors (x-axis). Additionally, the brightness (y-axis) and shower membership (symbols) are depicted.

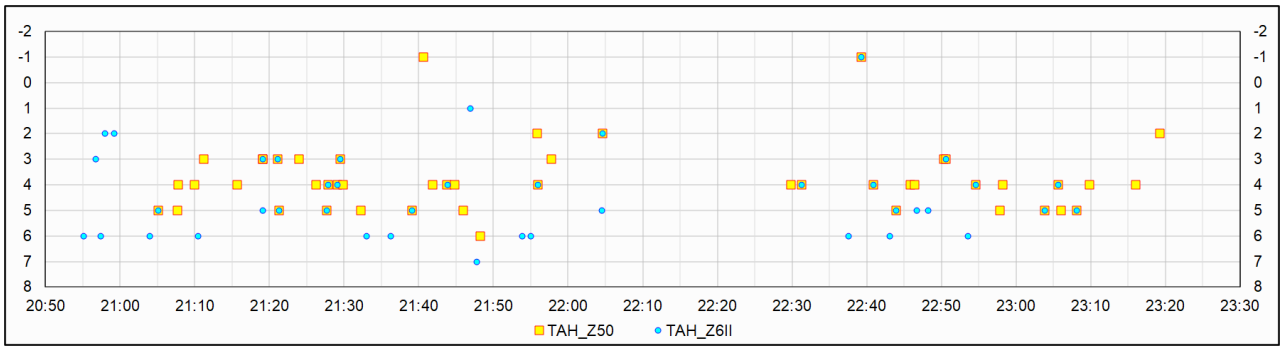

Figure 4 – Temporal distribution of TAH meteors separated for both cameras (x-axis). Additionally, the brightness (y-axis) is depicted.

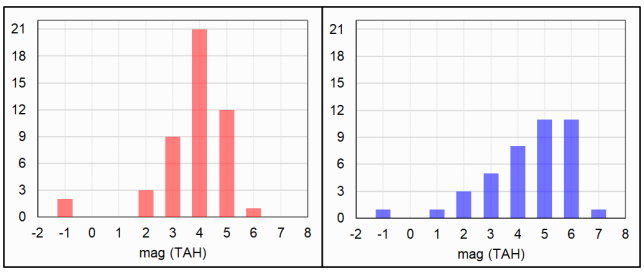

Figure 5 – Brightness distribution for both cameras separated.

5.2 Distribution by Duration

Since the camera is recoding the sky continuously without gaps (25 fps with 1/25 s integration time), I could determine the meteor duration accurately.

Figure 6 shows the distribution of meteor duration over meteor magnitude for both cameras, separated for TAH and other meteors.

In contrast to ANT and SPO, the duration of meteors from the slow TAH meteor shower decreases rapidly with lower brightnesses. That could be another reason to miss faint meteors.

5.3 Temporal Distribution of Meteors

The next diagrams show individual meteors without their brightness to improve the visibility of the temporal distribution.

To determine an hourly rate without ignoring short-term fluctuations in activity, I calculated the values as follows:

- sliding means of 10 min counts, multiplied by six (dotted lines in Figure 7),
- sliding means of 1-minute counts (weights by distance: 0.164, 0.151, 0.117, 0.077, 0.042, 0.020, 0.008, 0.003, 0.001), multiplied by 60 (solid lines in Figure 7).

Both graphs are corrected for the radiant altitude. The solid and dotted lines agree well with respect to amplitude and shape.

5.4 Correction for Clouds

The orange boxes in Figure 8 mark the intervals, when the cameras were active. Due to the adventurous camera mount, the Z50 started later. The recording of the Z6II camera stopped earlier, because after I had switched the memory card and battery, skies overcast quickly.

The blue and red areas show the cloudiness in percent of FOV for both cameras. Unfortunately, the clouds where partly transparent and there was no clear division line between dissipating clouds and clear skies. I tried to cope with that by ignoring some dissipating clouds. That seemed to be the best solutions, give that meteors were clearly visible even in denser parts of the cloud.

In Figure 9 I corrected the meteor activity for cloudiness. The dotted line are identical to the solid lines from Figure 7 (sliding means of 1-minute counts). The solid lines are the result when correcting for the cloud coverage.

If we compare the graphs for both cameras, we see only moderate agreement. The differences could be due to the different observing directions and limiting magnitudes of the cameras.

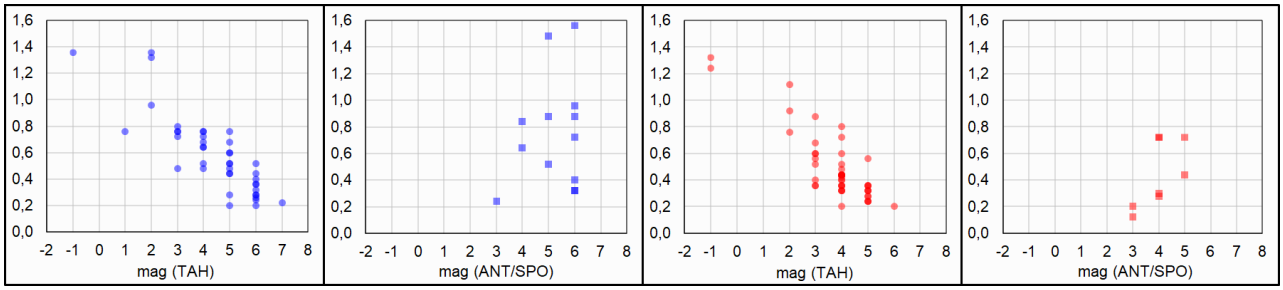

Figure 6 – Distribution of meteor duration versus brightness for both cameras, show separately for TAH and other meteors.

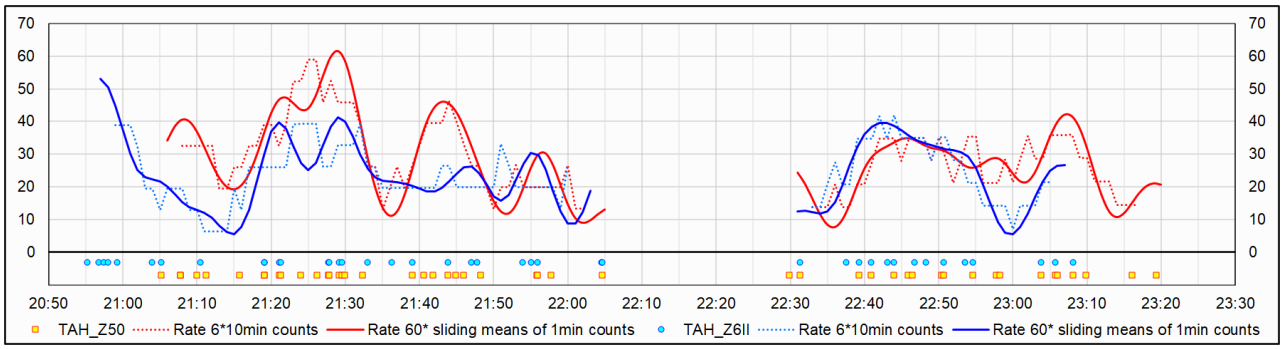

Figure 7 – Meteor detections and average hourly meteor rate of both cameras.

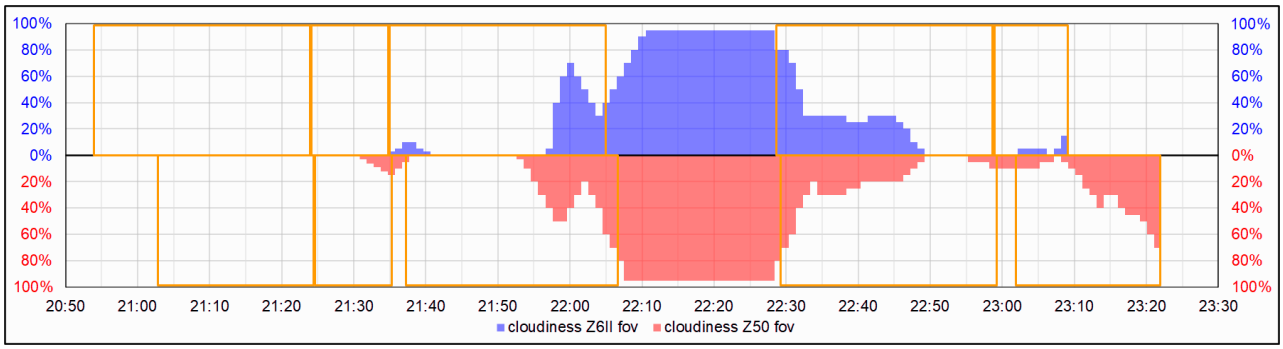

Figure 8 – Recording times of both cameras and cloudiness in their fields of view.

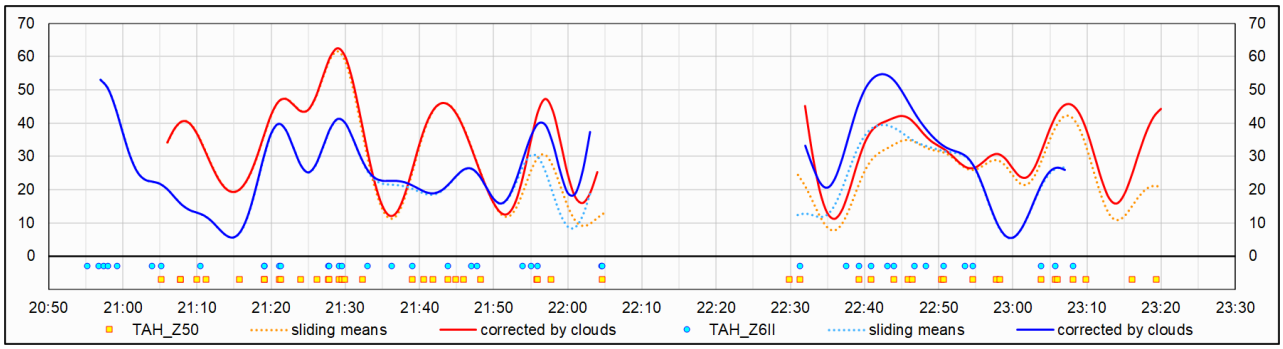

Figure 9 – Comparison of meteor rates from both cameras (dotted lines) and cloud-corrected rates (solid lines).

5.5 Field of View Correction

Given the location of the fields of view we could expect that the number of meteors of the Z50 cameras will be higher because of the larger atmospheric volume and the lower altitude. On the other hand, the weak TAH are further dimmed towards the horizon, which will reduce the number of detections. A correction seems not sensible.

The different sizes of FOV of 860 respectively 1909 square degrees were normalized to 1000 square degrees in Figure 10. The dotted lines are the cloud corrected sliding 1-minute means (identical to the solid lines in Figure 9). The solid lines are the same lines after FOV correction. The rates of the Z6II camera have slightly increased, whereas the counts of the Z50 camera are almost cut in half. Now the deviation between both graphs represents primarily the difference in limiting magnitude.

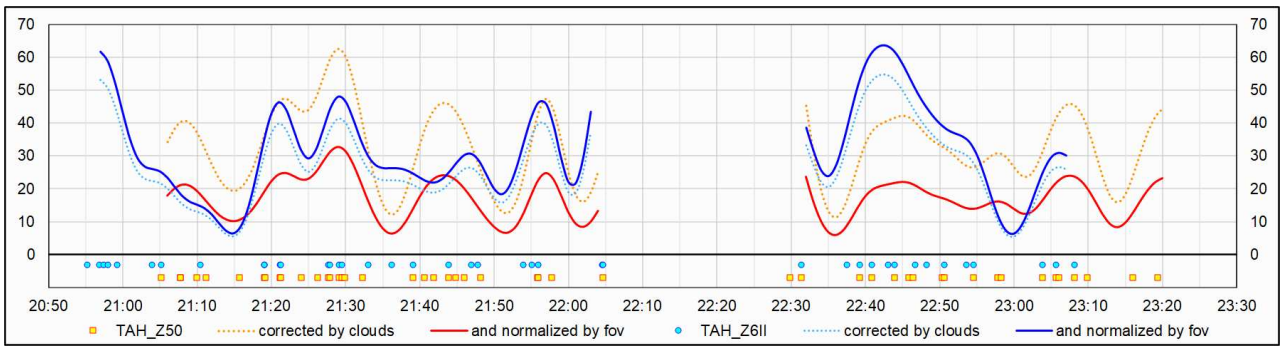

Figure 10 – Comparison of cloud-corrected meteor rate from both cameras (dotted lines), normalized to 1000 square degrees field of view (solid lines).

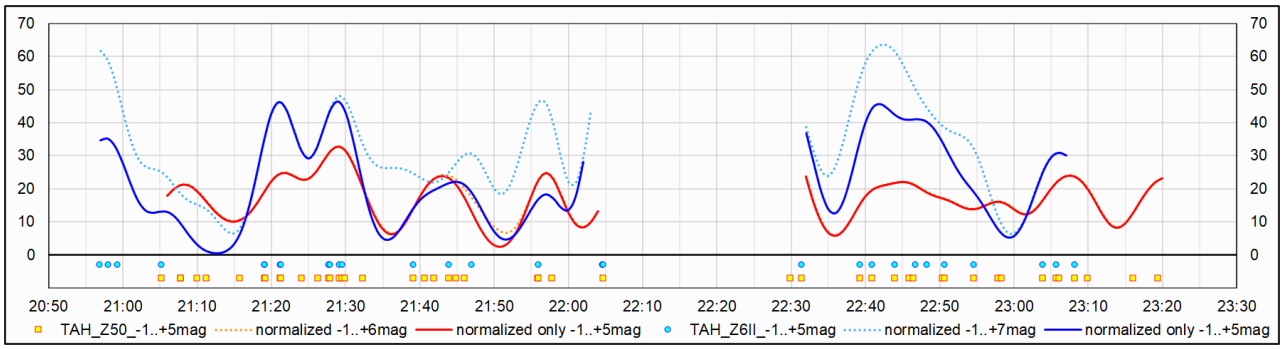

Figure 11 – Comparison meteor rate from both cameras with same correction as in Figure 10, but omitting meteors fainter than +5 mag.

5.6 Correction for Limiting Magnitude

Once more, the dotted lines in Figure 11 are the same as the solid lines in Figure 10. They incorporate meteors of all magnitudes from both cameras. The solid lines are calculated in the same way, but including only meteors of +5 mag and brighter.

Now the graphs agree much better. Activity gaps are visible in both cameras. The "missing" meteors of the Z6II camera near $21^{h}11^{m}$ and $23^{h}00^{m}$ UT are eye-catching.

However, there are also times when the two graphs deviate significantly. Reason could be the partial cloud cover at certain times, and that the fov was not fully overlapping. The fields of view of the two cameras make up for just 4.2 respectively 9.3 percent of the visible sky, but we could only expect to see the same rate of meteors if the entire sky was covered.

6 Summary

The analysis of video footage from the tau Herculids on May 30, 2022, shows the following results:

- The number of disturbing satellites crossing the field of view end of May at 52.5 deg north is embarrassing. There was hardly a minute without satellites, but up to ten satellites within one minute in the field of view.
- The short duration of the faint TAH meteors makes it difficult to detect them by visual observation on the monitor.
- The intervals without meteors agree in most cases. It remains unclear if that reflect real activity gaps or just random fluctuations given the small fields of view. Meteors in the larger FOV of the Z50 camera at times when the Z6II recorded nothing could be explained like this. For confirmation, we would need further data from cameras at other location with clear skies.
- The corrected hourly rates in normalized field of view of 1000 square degrees, taking also the radiant altitude and cloud coverage into account, yielded an average of 17 TAH per hour for the Z50 camera, and between 6 to 27 TAH per hour for individual 10 min intervals. 1000 square degree correspond to the FOV of a full-frame camera with a 45 mm lens.
- The corrected hourly rate of the Z6II camera was 32 TAH per hour with variations between 6 and 64 TAH per hour in 10 min intervals. If we omit meteors fainter than +5 mag, the numbers would reduce to 22 TAH per hour on average and 1 to 46 TAH per hour in 10-min intervals.
- The available data are not sufficient to calculate the population index – the number of meteors is too small, and the brightness estimation too inaccurate (in particular due to the clouds). For this, larger amounts of data are required and maybe software that can handle 4K video in mp4 format.

7 Acknowledgements

The author thanks Sirko Molau for helping with English translation.

Handling Editor: Javor Kac

Analysis of the unusual outburst of the τ-Herculids in 2022, observed from Arizona, USA

Thomas Weiland[1]

Based on a data sample of 141 visually observed τ-Herculid meteors, gathered under perfect conditions from Arizona, USA a moderate outburst with peak ZHRs of the order of 40–50, centred on $04^{\mathrm{h}}50^{\mathrm{m}}$ UT ($\lambda_{\odot} = 69\,^{\circ}\!.44$; eq. 2000.0) is confirmed. Highest activity lasted for ~ 1.3 h ($\lambda_{\odot} = 0\,^{\circ}\!.06$), resembling more a plateau rather than a distinct peak in shape. Population indices during the outburst varied greatly between $r = 2.3$ and 2.9, either indicating mass segregation within the stream or a blend with older dust. The appearance of (short) trains and the preponderance of orange to yellow colours both hints at fragile cometary material with a high amount of sodium.

Received 2022 August 17

1 A unique opportunity

Without doubt, it seems rather unusual if the break-up of a comet leads to a meteor outburst within a relatively short period of life. That was the forecast with the τ-Herculid meteor shower in 2022 which stayed almost absent in the sky for nearly a century. Its parent comet, 73P/Schwassmann-Wachmann 3 (SW3), discovered in 1930 as a member of the Jupiter family of comets (orbital period 5.4 years), underwent a multiple break-up in the autumn of 1995, resulting in a dramatic increase in brightness by more than six magnitudes. Thus, despite its modest diameter ($\sim$ 1.3 km after the break-up), a considerable expulsion of dust in the wake of the fragmentation was assumed (Lüthen et al., 2001). In the same study it was pointed out that Earth might interact with the dust trail formed in 1995 and a close encounter (0.0004 au distance) predicted for 2022 May 31, $04^{\mathrm{h}}55^{\mathrm{m}}$ UT ($\lambda_{\odot} = 69\,^{\circ}\!.44$). Further works either suppressed the possibility for enhanced activity (e.g. Wiegert et al., 2005; based on the Vaubaillon ejection model) or supported the prospect of an outburst (e.g. Horii et al., 2008; peak time $04^{\mathrm{h}}59^{\mathrm{m}}$ UT). Recent simulations performed by Rao (2021) agreed with both options, depending on the used parameters. Accordingly, estimates of the peak ZHR also varied widely, ranging from zero to storm level. As Earth was determined to pass the descending node of SW3 65.9 days *prior* to the arrival of the comet (Rao, 2021), the crucial question was whether the ejection velocity, size and number of particles released five revolutions ago was large enough to produce a discernible trail of dust finally ending up *ahead* of the comet. At least, those studies favouring the possibility of an outburst were convergent regarding the peak time (May 31, $\sim 05^{\mathrm{h}}$ UT) and the extremely low entry velocity of the meteoroids ($V_{\infty} \sim 12.5$ km/s; increased by about 4 km/s due to the gravity of the Earth), probably delivering mainly weak meteors of short duration.

[1]Ospelgasse 12-14/6/19, 1200 Wien, Austria.
Email: thomas.weiland@aon.at

IMO bibcode WGN-503–4-weiland-tah
NASA-ADS bibcode 2022JIMO...50..105W

2 Heading for the outburst

Fortunately, New Moon on May 30, $11^{\mathrm{h}}30^{\mathrm{m}}$ UT would leave skies dark and assist in spotting short and faint streaks of light. According to the predicted peak time, much of North America (except for the northwestern and northern part), Central and northwestern South America were the regions of the world best suited to pursue the event. Including the prospects of most promising weather, the southwestern United States, particularly Arizona, seemed the place to go (probability of clear skies at least 70%). As a further benefit, the semi-deserts of the Southwest offered the highest possible radiant elevation ($> 80°$), which would reduce the effect of the zenith attraction to a minimum, too.

Finally, a lonely area near Seligman, Arizona ($112°52'09''$ W, $35°16'32''$ N, 1590 m a. s. l.) was chosen as an observation site. Meteor watch commenced at $03^{\mathrm{h}}45^{\mathrm{m}}$ UT; by that time the Sun had already dropped 12° below the horizon and the radiant gained an elevation of $h_R = 74°$ (later rising to 82°). Conditions turned out to be perfect, presenting no clouds in the sky and decreasing wind, but with temperatures going down to 1 °C in the course of the night it got quite cold by Arizona standards. Limiting stellar magnitudes started out with $lm = 5.7$ and were improving to the remarkable value of 6.6 after twilight had ended (Table 1).

Surprisingly, the τ-Herculids (TAH) were active from the beginning, yielding 7 counts between $03^{\mathrm{h}}45^{\mathrm{m}}$ and $03^{\mathrm{h}}55^{\mathrm{m}}$ UT and 6 during the following 10-minute interval. Most TAH members appeared as short streaks in the sky, radiating from a rather large area (assumed $\sim 20°$ ⌀) northwest of α Bootis, as predicted (Rao, 2021). Hopes were high for a further increase in number which actually took place (13 TAH logged between $04^{\mathrm{h}}05^{\mathrm{m}}$ and $04^{\mathrm{h}}15^{\mathrm{m}}$ UT), obviously not only as an effect of the now completely dark sky. At least two times TAH meteors lit up simultaneously (i.e. at least two stream members within 2 seconds) and shortly thereafter they became somewhat brighter (up to -1 magnitude), mainly showing yellow to orange tints. In the further course, observed rates per 10 minutes hovered around 6–9, not giving way to a significant peak. This should not happen either at the predicted time, as somewhat higher 10-minute counts up to 12 were taking turns with lulls of only 4–5. Nevertheless, one of the

Table 1 – Magnitude distribution and population indices of 141 τ-Herculids logged on 2022 May 30/31.

Shower	UT	lm	−3	−2	−1	0	+1	+2	+3	+4	+5	Σ	r
TAH	03:45–04:45	6.41	0	0	3	4	3	4	13	11	8	46	2.29 ± 0.34
TAH	04:45–05:45	6.60	0	1	1	0	2	6	8	10	20	48	2.84 ± 0.54
TAH	05:45–06:45	6.60	1	0	2	1	2	4	1	8	10	29	2.34 ± 0.51
TAH	06:45–07:45	6.60	0	0	0	0	3	0	2	5	6	16	2.89 ± 1.44
Σ			1	1	6	5	11	14	24	35	44	141	
Mean		6.55											2.50 ± 0.21

most beautiful TAHs (magnitude −2) appeared around $05^{h}05^{m}15^{s}$ UT, this time of white-blue colour with train, travelling on a 20–25° long path from northeastern to western Leo. After $05^{h}55^{m}$ UT rates dropped dramatically (1 per 10 minutes each during the next two 10-minute intervals), only to perform a steep rise to 11 per 10 minutes between $06^{h}15^{m}$ and $06^{h}25^{m}$ UT again. That interval also saw the brightest TAH of the entire night ($06^{h}23^{m}30^{s}$ UT), a needle-like "shooting star" of magnitude −3, turning up in Ophiuchus on a 15° long path and sporting a yellow-orange colour with train. Eventually, the τ-Herculids were losing strength, ending up at 1–2 counts per 10 minutes; no more members with negative magnitudes were seen. At $07^{h}55^{m}$ UT the observation ended ($h_R = 51°$).

During 4.14 hours of effective observing time 141 TAH had been logged, together with 2 Antihelion meteors (ANT) and 32 sporadics (SPO).

3 Observing method and data analysis

Fieldwork was carried out as a single visual observation. For determination of the limiting magnitudes direct vision in combination with averted view was performed.

Population indices were derived using the magnitude difference between the meteors and the limiting stellar magnitudes, based on table 7.2, p. 122 and the table on p. 124 in the *Handbook for Meteor Observers* (Rendtel & Arlt, 2014).

ZHR calculations followed the procedure given in the *Handbook for Meteor Observers* (Rendtel & Arlt, 2014). The zenith exponent was assumed to be $\gamma = 1.0$. No perception coefficient was applied.

4 Results

4.1 Magnitude distribution

In general, the magnitude distribution of the 2022 τ-Herculids fits a standard function, steadily rising in number towards the +5-magnitude class, the latter probably an effect because of the exceptionally dark skies (Table 1 and Figure 1).

Only 6% of the recorded TAH, much less than compared to major annual streams, fell within the negative magnitude range; the bulk (94%) equalled magnitude 0 or fainter. No fireballs (magnitude −4 or brighter) were observed. The percentage of faint meteors (magnitudes +4 and +5) amounted to 56%.

As for SPO, only one meteor with negative magnitude was recorded (3%), equalling −2. The bulk of the SPO (59%) turned out to be faint (magnitude +4 and +5). The two ANT recorded reached magnitude 0 and +3, respectively.

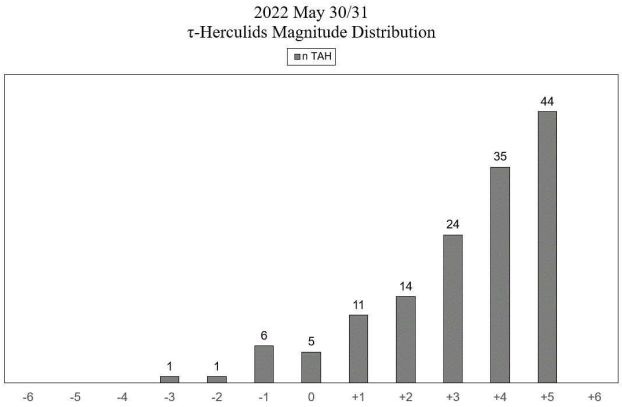

Figure 1 – Magnitude distribution of 141 τ-Herculids logged on 2022 May 30/31.

4.2 Population indices

Calculation of the population indices revealed a varying pattern (Table 1); during the first observing hour ($03^{h}45^{m}$ to $04^{h}45^{m}$ UT) an r-value of 2.29 ± 0.34 was determined, followed by a steep rise to $r = 2.84 \pm 0.54$ between $04^{h}45^{m}$ and $05^{h}45^{m}$ UT, mainly because of the preponderance of faint meteors (magnitudes +4 and +5). The third observing hour ($05^{h}45^{m}$ to $06^{h}45^{m}$ UT), coinciding with the brightest TAH of magnitude −3 (see Section 2), yielded a significantly lower r-value of 2.34 ± 0.51 again. Due to the fact that no more TAHs with negative magnitudes were logged between $06^{h}45^{m}$ and $07^{h}45^{m}$ UT, the population index once more went up to $r = 2.89 \pm 1.44$.

For the entire observing period the mean comes to $r = 2.50 \pm 0.21$, exactly matching the value used in order to generate the IMO ZHR Live Graph (`www.imo.net`, accessed 2022 August 11).

For comparison, calculation of the population index of the sporadic background (including ANT) resulted in a mean r of 2.73 ± 0.65.

Although the r-values given above are more or less suffering from large error widths, depending on the underlying meteor numbers, they reflect the impression of the observer in the field. Additionally, the average population index found for the sporadic background is quite in accordance with the mean value of ~ 2.84 given for the period of $\lambda_{\odot} \sim 50$–100° in Figure 1.11, p. 14 of the *Handbook for Meteor Observers* (Rendtel & Arlt, 2014). Thus, and because of the fact that observing conditions

did not change after 04^h10^m UT, the r-values obtained for the TAH are regarded to be real.

4.3 ZHR profile

As the limiting stellar magnitudes were close to the standard sky ($lm = 6.5$), it seems justified to employ the mean r-value of 2.50 (see Section 4.2), instead of individual population indices, for ZHR calculation.

Corresponding to the highest 10-minute count of 13 between 04^h05^m and 04^h15^m UT (see Section 2), the first observing hour (03^h45^m to 04^h45^m UT) yielded a ZHR-value of 52 ± 8. Afterwards, despite further comparable 10 minute-counts from time to time and the fact of the radiant still rising until $\sim 04^h50^m$ UT, ZHRs were continuously declining from 44 ± 6 between 04^h45^m and 05^h45^m UT to 17 ± 4 between 06^h45^m and 07^h45^m UT (Figure 2).

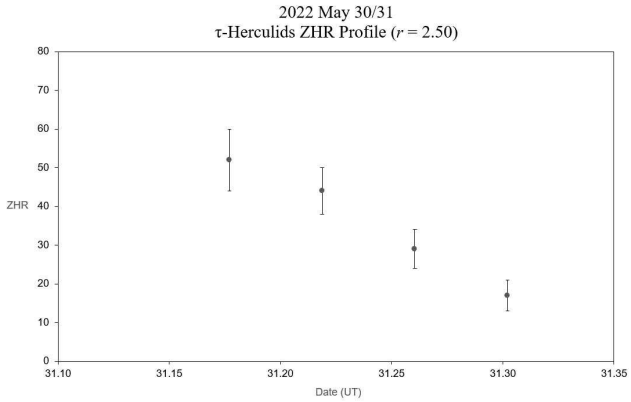

Figure 2 – τ-Herculids ZHR profile on 2022 May 30/31.

In order to resolve the activity profile more precisely, ZHR-values based on 10-minute intervals and the average population index of $r = 2.50$ (see Section 4.2) have been calculated. This naturally results in larger fluctuations (Figure 3), particularly at the start of the observation. Nevertheless, three peaks (around May 31.17, 31.23 and 31.26) become visible, approximately coinciding with the highest proportion of bright meteors (< magnitude 0) and simultaneous events.

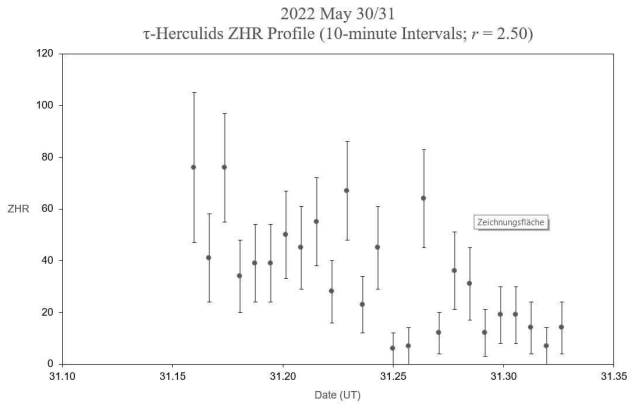

Figure 3 – τ-Herculids ZHR profile on 2022 May 30/31, based on 10-minute intervals.

To smooth the profile, in a third step ZHR-values were averaged using a sliding mean of five bins per step (A5), yielding the activity curve seen in Figure 4. This reveals a plateau between May 31.17 and 31.23 (04^h05^m to 05^h35^m UT) with ZHRs fluctuating around 40–50, followed by a less pronounced sub-peak around May 31.27 (06^h35^m UT) with a ZHR of 30.

Although the activity level given in Figure 4 seems to be quite in agreement with the corresponding IMO ZHR Live Graph (page generated on 2022 August 11; `www.imo.net`), the profile differs somewhat in shape, as the plateau obviously does not come out in the Live Graph. Instead, the latter shows a distinct peak around 05^h15^m UT. Likewise, the sub-peak around 06^h35^m UT is only indicated in the Live Graph, too.

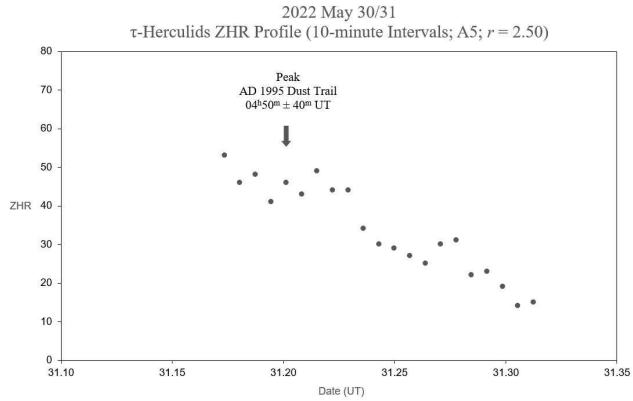

Figure 4 – τ-Herculids ZHR profile on 2022 May 30/31, based on 10-minute intervals averaged over 5 bins (A5).

4.4 Appearance of the τ-Herculids in the sky

Pursuing the outburst of the τ-Herculids offered a rare opportunity to observe meteors recently released from a broken comet.

As assumed, quite a high percentage of the TAHs (8.5%) lit up as short streaks of light (< 3°), also far from the radiant; this was not confined to faint meteors, as 50% of them belonged to the +1- to +3-magnitude class. On the other hand, even the brightest TAHs did not show a path longer than 25°.

6.4% of the τ-Herculids resembled travelling stars, without any hint of a wake, only observed with meteors of magnitude 0, +2 and +3 (Tables 2 and 3). Rather a high percentage (24.1%) left a short train behind, mainly in the +2- to +4-magnitude class, but also seen with TAHs of magnitude +5 and up to −1. Distinctive trains (8.5%) were observed in all magnitude classes except +5, showing their highest percentage with magnitudes −3 and −2 (100.0% each); as expected, they decrease towards fainter meteors. No persistent trains were registered which is also the case for flares and terminal bursts.

As for colours, the majority of the τ-Herculids with magnitude 0 or brighter exhibited orange (46.2%) and yellow (30.8%) colours, together with white (19.2%) and bluish tints to a much lesser extent (3.9%).

5 Discussion

There is no doubt that the outburst of the 2022 τ-Herculids was mainly caused by dust released during

Table 2 – Train distribution on 2022 May 30/31 (%-values refer to the total TAH number recorded (Σ TAH) and %-values per magnitude range refer to the number of TAH within each type of trains).

Type of train	Σ TAH	Magnitude range	< 0	≥ 0
		% (number per type = 100)		
Star-like (no train)	6.4	Star-like (no train)	0.0	100.0
Short trains	24.1	Short trains	5.9	94.1
Trains	8.5	Trains	33.3	66.7

Table 3 – Train distribution on 2022 May 30/31 (%-values per magnitude class refer to the number of TAH logged in each class).

Magnitude class	−3	−2	−1	0	+1	+2	+3	+4	+5
% (number per class = 100)									
Star-like (no train)	0.0	0.0	0.0	40.0	0.0	28.6	12.5	0.0	0.0
Short trains	0.0	0.0	33.3	0.0	18.2	35.7	50.0	28.6	6.8
Trains	100.0	100.0	33.3	20.0	27.3	7.1	4.2	5.7	0.0

the 1995 break-up of comet 73P/Schwassmann-Wachmann 3. Assuming that their activity was no higher before $03^{\mathrm{h}}45^{\mathrm{m}}$ UT than after, which is suggested by the IMO ZHR Live Graph, too, ZHRs were peaking around $04^{\mathrm{h}}50^{\mathrm{m}} \pm 40^{\mathrm{m}}$ UT ($\lambda_\odot = 69\,\overset{\circ}{.}44 \pm 0\,\overset{\circ}{.}03$; eq. 2000.0) at the order of 40–50, almost matching the prediction of Lüthen et al. (2001) and Horii et al. (2008) (see Section 1). In this context it seems secondary whether there was a sharp peak or just a plateau; no forecast based on optical meteors (summarized in Ye and Vaubaillon, 2022) differs from the above time by more than 80 minutes ($\Delta\lambda_\odot = 0\,\overset{\circ}{.}05$); estimated ZHRs range from 22 to 76, in one case to 600+.

The reason for the indicated sub-peak around $06^{\mathrm{h}}35^{\mathrm{m}}$ UT ($\lambda_\odot = 69\,\overset{\circ}{.}51$), however, is not clear at the moment. One might think of higher particle densities within the 1995 trail or an overlapping concentration of older dust. Since the main peak falls into a period with a lower population index, too (see Section 4.2), r-values seem not to be helpful to differentiate between the two possibilities. In any case, the appearance of the brightest TAH at $06^{\mathrm{h}}23^{\mathrm{m}}30^{\mathrm{s}}$ UT (see Section 2), together with a fireball of magnitude −8 at $06^{\mathrm{h}}31^{\mathrm{m}}$ UT seen and imaged by other observers in the southwestern USA (`www.imo.net`) slightly favours the probability of older dust.

Although the lack of persistent trains, flares and terminal bursts does not support fragile cometary material at a glance, for further interpretation one has to take the extremely low entry velocity into account. In this context, the relatively high percentage ($\sim 33\%$) of TAHs leaving (short) trains behind speaks quite well for particles with lower bulk density compared to other annual streams.

As the vast majority ($\sim 77\%$) of TAHs with at least magnitude 0 showed orange to yellow tints, which provides an indication of sodium, one might further deduce that the meteoroids were neither strongly heated up nor modified by space weathering for a long time.

6 Conclusion

In summary, it can be concluded that the τ-Herculids delivered a modest outburst in 2022 (peak ZHRs of the order of 40–50), centred on $04^{\mathrm{h}}50^{\mathrm{m}}$ UT ($\lambda_\odot = 69\,\overset{\circ}{.}44$; eq. 2000.0), with the highest level lasting for about 1.3 h ($\lambda_\odot = 0\,\overset{\circ}{.}06$). Population indices during the outburst varied greatly between $r = 2.3$ and 2.9, either indicating mass segregation within the stream or overlapping older dust. The relatively high percentage of (short) trains and the predominance of orange to yellow colours points to fragile cometary material with a high amount of sodium.

References

Horii S., Watanabe J.-I., and Sato M. (2008). "Meteor Showers Originated from 73P/Schwassmann Wachmann". *Earth, Moon, and Planets*, **102:1-4**, 85–89.

Lüthen H., Arlt R., and Jäger M. (2001). "The Disintegrating Comet 73P/Schwassmann-Wachmann 3 and Its Meteors". *WGN, Journal of the International Meteor Organization*, **29:1**, 15–28.

Rao J. (2021). "Will Comet 73P/Schwassman-Wachmann 3 produce a meteor outburst in 2022?". *WGN, Journal of the International Meteor Organization*, **49:1**, 3–14.

Rendtel J. and Arlt R., editors (2014). *Handbook for Meteor Observers*. International Meteor Organization, Potsdam.

Wiegert P. A., Brown P. G., Vaubaillon J., and Schijns H. (2005). "The τ Herculid meteor shower and Comet 73P/Schwassmann-Wachmann 3". *MNRAS*, **361:2**, 638–644.

Ye Q. and Vaubaillon J. (2022). "The 2022 encounter of the outburst material from comet 73P/Schwassmann-Wachmann 3". *MNRAS*, **515:1**, L45–L49.

Handling Editor: Javor Kac

The International Meteor Organization

www.imo.net

Follow us on Facebook InternationalMeteorOrganization

Follow us on Twitter @IMOMeteors

Council

President: Cis Verbeeck,
Bogaertsheide 5, 2560 Kessel, Belgium.
e-mail: cis.verbeeck@gmail.com

Vice-President: Juraj Tóth,
Fac. Math., Phys. & Inf., Comenius Univ.,
Mlynska dolina, 84248 Bratislava, Slovakia.
e-mail: toth@fmph.uniba.sk

Secretary-General: Robert Lunsford,
14884 Quail Valley Way, El Cajon,
CA 92021-2227, USA. tel. +1 619 755 7791
e-mail: lunro.imo.usa@cox.net

Treasurer: Marc Gyssens, Heerbaan 74,
B-2530 Boechout, Belgium.
e-mail: marc.gyssens@uhasselt.be
BIC: GEBABEBB
IBAN: BE30 0014 7327 5911
Bank transfer costs are always at your expense.

Other Council members:
Karl Antier, 16, rue de la République,
F-04100 Manosque, France.
e-mail: karl.antier@gmx.fr
Javor Kac (see details under WGN)
Detlef Koschny, Zeestraat 46,
NL-2211 XH Noordwijkerhout, Netherlands.
e-mail: detlef.koschny@esa.int
Sirko Molau, Abenstalstraße 13b, D-84072
Seysdorf, Germany. e-mail: sirko@molau.de
Francisco Ocaña Gonzalez, C/ Arquitectura, 7.
28005 Madrid, Spain.
e-mail: francisco.ocana.gonzalez@gmail.com
Vincent Perlerin, 16, rue Georges Bernanos,
51100 Reims, France.
e-mail: vperlerin@gmail.com
Jürgen Rendtel, Eschenweg 16, D-14476
Marquardt, Germany. e-mail: jrendtel@aip.de

Commission Directors

Visual Commission: Jürgen Rendtel
Generic e-mail address: visual@imo.net
Electronic visual report form:
http://www.imo.net/visual/report/electronic
Video Commission: Sirko Molau (video@imo.net)
Photographic Commission: Bill Ward
(bill_meteor@yahoo.com)
Generic e-mail address: photo@imo.net
Radio Commission: Chris Steyaert
(radio@imo.net)
Fireballs: Online fireball reports:
http://fireballs.imo.net

Webmaster

Karl Antier, e-mail: webmaster@imo.net

WGN

Editor-in-chief: Javor Kac
Na Ajdov hrib 24, SI-2310 Slovenska Bistrica,
Slovenia. e-mail: wgn@imo.net;
include METEOR in the e-mail subject line

Editorial board: Ž. Andreić, D.J. Asher,
F. Bettonvil, M. Gyssens, C. Hergenrother,
T. Heywood, J. Rendtel, C. Verbeeck,
S. de Vet, D. Vida.

IMO Sales

Available from the Treasurer or the Electronic Shop on the IMO Website	€	$
IMO membership, including subscription to WGN Vol. 50 (2022)		
Surface mail	26	32
Air Mail (outside Europe only)	49	60
Electronic subscription only	21	25
Proceedings of the International Meteor Conference on paper		
1990, 1991, 1995, 1996, 1999, 2000, 2002, 2003, per year	9	12
2007, 2010, 2011, per year	15	20
2012, 2013, 2015, 2017 per year	25	32
Proceedings of the Meteor Orbit Determination Workshop 2006	15	20
Radio Meteor School Proceedings 2005	15	20
Handbook for Meteor Observers	23	29
Meteor Shower Workbook	12	16
Electronic media		
Meteor Beliefs Project ZIP archive	6	8

Bright pre-maximum Perseid from Slovenia

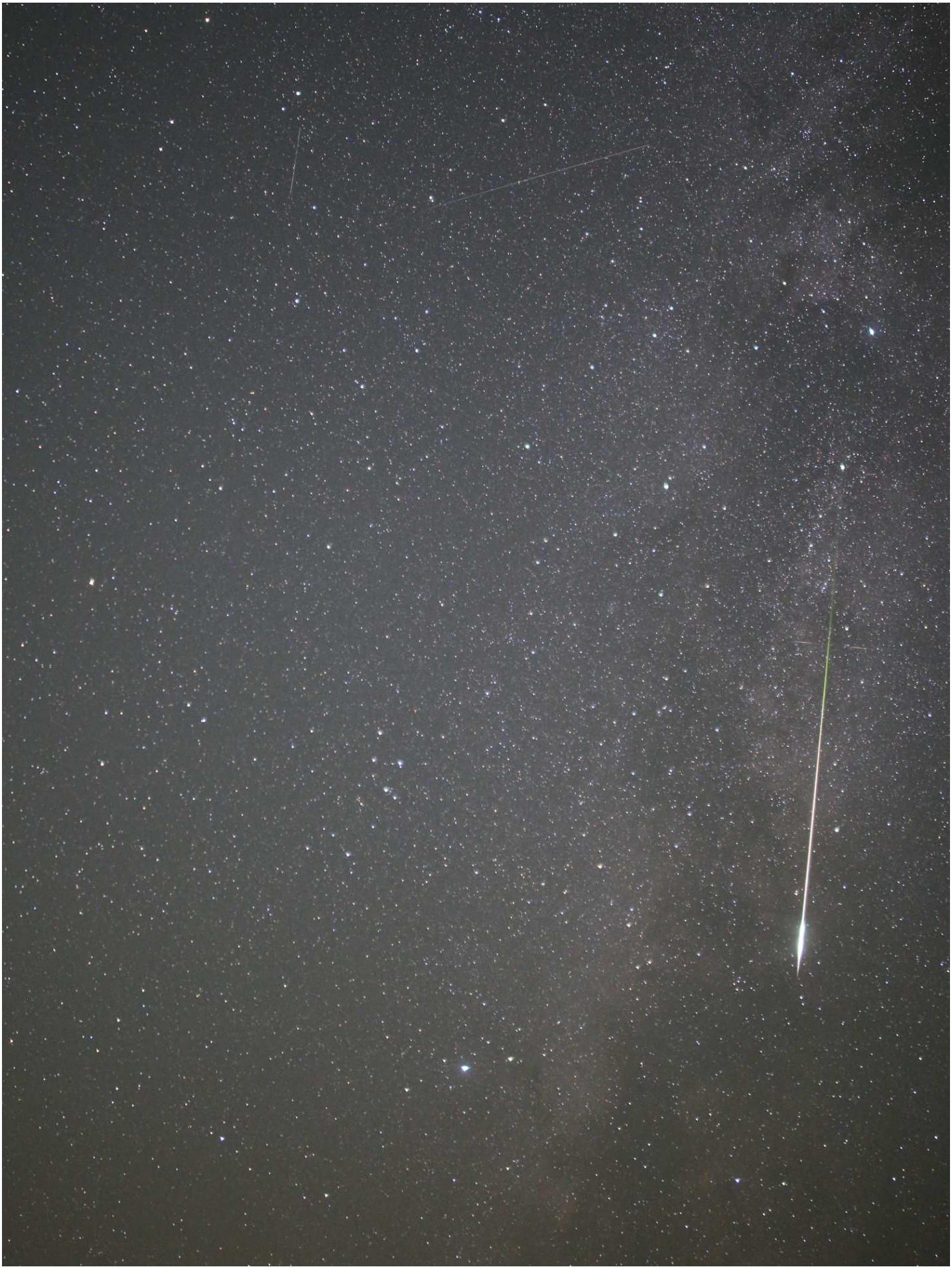

This bright Perseid was photographed on 2022 August 7, at $01^{\mathrm{h}}01^{\mathrm{m}}$ UT from Grmada, Slovenia. Canon 6D camera was employed with 24-mm $f/1.4$ lens and 15 s exposure at ISO 3200. The persistent train was visible on photographs for 7 minutes. Photo courtesy: Javor Kac.